https://doi.org/10.5194/egusphere-2025-4028
Preprint. Discussion started: 16 September 2025

Driving mechanisms of the dissolved oxygen budget in the Levantine Sea: a coupled physical-biogeochemical modelling approach

Joelle Habib[1,2,3], Caroline Ulses[1], Claude Estournel[1], Milad Fakhri[3], Patrick Marsaleix[1], Thierry Moutin[4], Dominique Lefevre[4], Mireille Pujo-Pay[5], Marine Fourrier[2], Laurent Coppola[2,6], Cathy Wimart-Rousseau[7] and Pascal Conan[5,6†]

[1]Laboratoire d'Etudes en Géophysique et Océanographie Spatiales (LEGOS), Université de Toulouse, CNES/CNRS/IRD/UT3, 14 avenue Edouard Belin, 31400 Toulouse, France
[2]Sorbonne Université, CNRS, Laboratoire d'Océanographie de Villefranche, LOV, 06230 Villefranche-sur-Mer, France
[3]National Center for Marine Sciences, National Council for Scientific Research (CNRS-L), Jounieh, Lebanon
[4] Aix Marseille Univ, Université de Toulon, CNRS, IRD, MIO, Marseille, France
[5]Laboratoire d'Océanographie Microbienne (LOMIC), CNRS, UMR 7621, Sorbonne Université, 1 Avenue Pierre Fabre, 66651 Banyuls-sur-mer, France
[6]Sorbonne Université, CNRS OSU STAMAR – UAR2017, 4 Place Jussieu, 75252 Paris, France
[7]National Oceanography Centre Southampton, European Way, Southampton, SO14 3ZH, UK

[†] Deceased

Correspondence to: Joelle Habib (joellehabib22@hotmail.com)

Abstract.

The Levantine Basin is an ultra-oligotrophic region and the formation site of the Levantine Intermediate Waters. For the first time, a high-resolution 3D coupled hydrodynamic-biogeochemical model, SYMPHONIE-Eco3MS, was used to investigate the seasonal and interannual variability of dissolved oxygen (O_2) in the Levantine Basin and estimate its basin-wide budget for the period 2013–2020. Our results show that the simulated O_2 concentrations align well with *in situ* data from research cruises and Argo floats. During winter, the surface layer is undersaturated in oxygen by up to 2% across the entire basin, leading to atmospheric oxygen absorption. The model shows that on an annual scale, the basin acts as a net sink for atmospheric oxygen, with the Rhodes Gyre exhibiting uptake rates twice as high as the rest of the Levantine Basin. The surface layer also serves as a source of dissolved oxygen for intermediate depths, with 4.2 ± 1.1 mol m^{-2} $year^{-1}$ of dissolved oxygen vertically transported. Oxygen is transported laterally into the basin from the Ionian Sea and exported towards the Aegean Sea, with winter heat loss intensity enhancing this lateral export at both surface and intermediate layers. The Levantine Basin alternates between autotrophic and heterotrophic states, depending on the intensity of winter surface heat loss. Spatially, the Rhodes Gyre emerges as a significant oxygen pump, contributing 41% of the total oxygen production in the surface layer in the Levantine basin. This study highlights the need for further modeling studies on pluri-annual and multi-decadal scales to explore the interannual

https://doi.org/10.5194/egusphere-2025-4028
Preprint. Discussion started: 16 September 2025

variability and evolution of the annual oxygen budget across the entire Eastern Basin, particularly in the context of climate change.

1 Introduction

Dissolved oxygen (O_2) is essential for marine life, supporting respiration of living organisms and the oxidation of organic matter, and therefore influencing the biogeochemical cycles of important elements in the ocean. The ocean's oxygen inventory is primarily controlled by photosynthesis, respiration of organic matter, remineralization, temperature and salinity-dependent oxygen solubility, air-sea exchange and the mixing and advective fluxes influencing the ventilation of water masses. Since 1960, the total oxygen inventory has decreased by 2% in the Global Ocean (Schmidtko et al., 2017). This decrease in oxygen inventory referred to as deoxygenation has been attributed to the global warming which leads to the reduction of oxygen solubility, explaining ~15% of the current total global oxygen loss (Schmidtko et al., 2017), and the increase of upper ocean stratification generating a reduction of ventilation and circulation of deep ocean layers (Helm et al., 2011; Schmidtko et al., 2017). However, oxygen changes present large regional and temporal variability (Schmidtko et al., 2017; Stramma and Schmidtko, 2021). The decline in oxygen inventory induced by global warming, combined with seasonal, interannual, and decadal variations, is barely detectable in the upper layer of the water column. The description and assessment of the various drivers and processes influencing oxygen changes may provide valuable insight into the complex regional variations in oxygen dynamics.

The objective of the present work is to assess the main mechanisms controlling the oxygen changes and budget in the ultra-oligotrophic south-eastern Mediterranean Sea at seasonal and interannual time scales over 7 years. The Mediterranean Sea is a well-ventilated basin compared to the World Ocean (Schneider et al., 2014; Tanhua et al., 2013). The low salinity Atlantic Water (AW) enters the surface layer through the Gibraltar Strait and travels towards the eastern sub-basin. It gradually transforms into a more saline Mediterranean Water due to the air-sea heat and moisture fluxes (Malanotte-Rizzoli et al., 2014). Reaching the Levantine Basin (Fig. 1), the Modified AW (MAW) subducts under the warm and saline Levantine Surface Water (LSW) in summer. During winter, surface heat loss increases water density, triggering vertical mixing that reaches intermediate depths and leads to the formation of the Levantine Intermediate Water (LIW). The Rhodes Gyre, a permanent cyclone in the northwest of the Levantine Basin (Lascaratos et al., 1999; Lascaratos and Nittis, 1998; Sur et al., 1993), has been identified as the main area of LIW formation. Then, LIW propagates between 200-600 m in the whole Mediterranean (Brasseur et al., 1996). This water impacts the deep water formation in both the Adriatic Sea (Gačić et al., 2010; Lascaratos et al., 1999) and the Gulf of Lion (Schneider et al., 2014), acting as a preconditioning factor for these water formations with its high salinity. Part of LIW also exits the Mediterranean Sea, flowing toward the Atlantic.

The Levantine Basin is considered an ultra-oligotrophic region, except the Rhodes Gyre, where winter vertical convection enriches the surface layer with nutrients, stimulating organic carbon production (D'Ortenzio et al., 2021; Lavigne et al., 2013) and its export to the intermediate and surrounding areas (Habib et al., 2023). Previous studies have investigated the oxygen distribution and dynamics in this region (Di Biagio et al., 2022; Klein et al., 2003; Manca et al., 2004; Mavropoulou et al., 2020; Schlitzer et al., 1991; Tanhua et al., 2013). The vertical distribution in the basin is characterized by a surface layer exhibiting seasonal variability. During the stratified period, the upper waters present an oversaturated surface water and a sub-surface oxygen maximum (235 µmol kg^{-1}) between 50-80 m (Di Biagio et al., 2022; Kress et al., 2003; Mavropoulou et al., 2020), attributed to various processes such as primary production

https://doi.org/10.5194/egusphere-2025-4028
Preprint. Discussion started: 16 September 2025

within that layer, or alternatively, downward transport mechanisms like subduction (Di Biagio et al., 2022). In winter, the oxygen vertical profile shows an upper mixed layer with maximum dissolved concentrations of 240 µmol kg^{-1}, characterised by an undersaturation in oxygen at the surface related to the atmosphere. At intermediate depths, the LIW oxygen has values ranging from 197 to 210 µmol kg^{-1} (Mavropoulou et al., 2020). An Oxygen Minimum Layer (OML) is located between 600-1200 m with a minimum concentration of 170/180 µmol kg^{-1} (Tanhua et al., 2013). Below this layer, deep waters originating from the Adriatic and Aegean seas present values above 185 µmol kg^{-1}, slightly higher than the ones recorded for the OML (Mavropoulou et al., 2020).

The Levantine Basin shows spatial changes in oxygen content occurring at short, annual, and decadal time scales (Kress et al., 2014; Sisma-Ventura et al., 2016). The modeling study by Cossarini et al. (2021) showed a negative trend in oxygen concentration at the surface of the Mediterranean Sea due to the surface temperature increase over the past two decades (Escudier et al., 2021; Ozer et al., 2016; 2022). Mavropoulou et al. (2020) highlighted a variability in deep and intermediate layers' oxygen concentration linked to shifts in the formation location of water masses between the Adriatic and the Aegean seas. In particular, in the 1990s, during the Eastern Mediterranean Transient (EMT), warmer, saltier, and more oxygenated waters originating from the Aegean Sea flowed into the deep layers of the Levantine Basin (Lascaratos et al., 1999). A net decrease in the oxygen inventory in deeper layers (1200-2000 m) of the southeastern Levantine Basin over the 20 years from 2002 to 2020 has also been pointed out by Sisma-Ventura et al. (2021), reflecting a return to pre-EMT state due to mixing between Aegean and Adriatic waters. To date, the oxygen inventory in the Eastern Mediterranean Basin remains poorly understood, with limited spatial and temporal observations in the Levantine Basin, and there is no proposed comprehensive budget quantification for the entire region. The PERLE (Pelagic Ecosystem Response to Deep Water Formation in the Levant Experiment) project aimed to gain insights into the biogeochemical cycles in this region through multi-platform observations and modelling. In this study, we quantify the seasonal and interannual variations in the oxygen inventory of the Levantine surface and intermediate water masses, detailing the contribution of air-sea oxygen fluxes, biological and physical processes. This analysis is based on 3D coupled hydrodynamic-biogeochemical model outputs covering a period of 7 years, from 2013 to 2020.

After the introduction (Sect. 1), this paper is organized as follows. Sect. 2 describes the coupled hydrodynamic-biogeochemical model implemented in the Levantine Basin and observations used for the model assessment. Sect. 3 first presents an assessment of the model results using *in situ* observations, then investigates the seasonal and interannual dynamics of oxygen in the surface and intermediate layers for the Levantine Basin, describes its spatial variability, and finally estimates an annual budget of oxygen. This section is followed by a discussion of the results and a conclusion in Sect. 4 and 5, respectively.

2. Material and Method

2.1 Modeling

2.1.1 The coupled hydrodynamic-biogeochemical model

The modeling presented in this study is based on the biogeochemical model Eco3M-S forced offline by the ocean circulation model SYMPHONIE, described in detail in Marsaleix et al. (2006, 2008), Estournel et al. (2016), and Damien et al. (2017). This latter is a 3D primitive equation model with a free surface and generalized sigma vertical

https://doi.org/10.5194/egusphere-2025-4028
Preprint. Discussion started: 16 September 2025

coordinate previously used to simulate the hydrodynamic conditions of the Mediterranean Sea: in river plumes (Estournel et al., 1997, 2001; Marsaleix et al., 1998), for dense water formation (Estournel et al., 2005, 2016; Herrmann et al., 2008; Ulses et al., 2008) and shelf-slope exchanges (Mikolajczak et al., 2020).

We used the biogeochemical model Eco3M-S, a multi-nutrient and multi-plankton functional type model, representing the dynamics of the pelagic plankton ecosystem and the cycles of carbon, nitrogen, phosphorus, silicon, and oxygen (Auger et al., 2011; Ulses et al., 2023). The phytoplankton is represented by three size classes: pico-, nano-, and micro-phytoplankton (named class 1, 2, and 3, respectively), with variable internal ratios. The zooplankton is also represented by three size classes: nano-, micro-, and mesozooplankton (named class 1, 2, and 3, respectively). A compartment of bacteria has been explicitly taken into account. The internal composition varies for phytoplankton and remains constant for heterotrophic organisms. Four dissolved inorganic nutrients have been considered: nitrate, ammonium, phosphate, and silicate. In addition to dissolved organic matter (DOM), particulate organic matter (POM) has been divided into two weight classes, namely light and heavy. The biogeochemical model was previously used to study the dynamics of the planktonic ecosystems and organic carbon (Auger et al., 2014; Herrmann et al., 2013; Kessouri et al., 2018; Many et al., 2021; Ulses et al., 2016), as well as the nitrogen and phosphorus cycles (Kessouri et al., 2017), and the oxygen dynamics (Ulses et al., 2021) in the northwestern Mediterranean Sea. The rate of change of dissolved oxygen concentration due to biogeochemistry in the water column is calculated based on the following equation:

$$\frac{dDOx}{dt} = \sum_{i=1}^{3}(GPP_i - RespPhy_i)\gamma_{C/DOx} - \sum_{i=1}^{3}(RespZoo_i)\gamma_{C/DOx} - RespBac\,\gamma_{C/DOx} + (UptPhy_{i,NO_3} - Nitrif)\gamma_{NH_4/DOx} \quad \text{(Eq. 1)}$$

The dissolved oxygen concentration is represented by the term DOx. GPP_i and $RespPhy_i$ are gross primary production and respiration, respectively, for phytoplankton group i. $RespZoo_i$ and RespBac are respiration of zooplankton group i and of bacteria, $UptPhy_{i,NO3,}$ and Nitrif uptake of nitrate by phytoplankton class i, and nitrification, respectively. $\gamma_{C/DOx}$ and $\gamma_{NH_4/DOx}$, equal to 1 and 2, respectively, are the moles of DOx used per mole of C in respiration and needed to oxidize one mole of ammonium in nitrification as described in Grégoire et al. (2008).

The flux of dissolved oxygen at the air-sea interface is governed by the following equation:

$$DOxFlux = Kw(DOxSat - DOxSurf) \quad \text{(Eq. 2)}$$

$DOxSat$ represents the oxygen saturation also known as solubility and $DOxSurf$ the concentration of dissolved oxygen at the surface. The dissolved oxygen at solubility level is determined using the Garcia and Gordon (1992) equation. The oxygen saturation anomaly (OSA, expressed in percentage) is defined as the difference between the dissolved oxygen concentration and the solubility: $(DOx - DOxSat)/DOxSat$ x100 %. Kw represents the O_2 transfer velocity in m s^{-1}. We used the parametrization of Wanninkhof and McGillis (1999) with a cubic dependency to the 10-m wind speed following the study of Ulses et al. (2021) in the northwestern Mediterranean deep convection area, which obtained the best fits with in situ observations of oxygen concentration using this parametrization.

https://doi.org/10.5194/egusphere-2025-4028
Preprint. Discussion started: 16 September 2025

2.1.2 Implementation

The implementation of the coupled physical-biogeochemical model was described in detail in Habib et al. (2023). The hydrodynamic model covers the Mediterranean Sea and the Marmara Sea and it extends to 8° west in the Gulf of Cadiz.The horizontal resolution varies between 2.3 and 4.5 km, in general. A narrowing was conducted in the Gibraltar Strait with a 1.3 km grid for a better representation of the exchange area between the Mediterranean Sea and the Atlantic Ocean. The model has 60 vertical vanishing quasi sigma levels (Estournel et al., 2021) with closer levels near the surface. The period simulated by the hydrodynamic model runs from May 2011 to May 2021. This model configuration was used to describe the surface and intermediate water circulations in the eastern Mediterranean Sea (Estournel et al., 2021). Atmospheric forcings were provided by the ECMWF model with a horizontal resolution of 1/8° using hourly fields (wind, air temperature and humidity, pressure, solar and downward longwave radiation, and precipitation). The model accounts for a total of 142 rivers (Fig. 1).

The biogeochemical model Eco3M-S was forced by daily fields of temperature, salinity, current, and vertical diffusivity from the SYMPHONIE model. It covers the period between August 2011 till March 2021. The two first years for the biogeochemical model were considered as a spin-up and were not considered in the analysis. We used wind speed and solar radiation atmospheric forcings provided by the ECMWF model as for the hydrodynamic simulation. The biogeochemical model was initialized using climatological fields of *in situ* nutrient and dissolved oxygen concentrations from the CARIMED (CARbon in the MEDiterranean Sea, Alvarez et al., 2019) database and Biogeochemical-Argo (BGC-Argo) float data over the 2011-2012 summer periods when data were available, in 10 sub-regions. At the river mouths, concentrations of nutrients were imposed by sub-basin using the dataset of Ludwig et al. (2010). Dissolved oxygen at river mouths was set at saturation values. In the Atlantic Ocean, nutrients were prescribed using monthly profiles from the World Ocean Atlas 2009 climatology at 5.5 °W. In the Marmara Sea, to represent a two-layer flow regime, we imposed a daily relaxation towards a nutrient concentration of 0.24 and 1.03 mmol N m^{-3} and a phosphate concentration of 0.06 and 0.05 mmol P m^{-3} for depths above and below 15 m, respectively, based on the observations near the Dardanelles Strait from (Tugrul et al., 2002).

2.1.3 Study area and budget calculation

The study area (delimited by the black lines, Fig. 1) covers 540 000 m^2. For spatial mean and budget calculation, the water column was divided into three layers based on the biogeochemical processes as well the depth of the LIW: the surface layer defined as the photic layer covering the surface to 150 m depth where photosynthesis takes place, the underlying intermediate layer from 150 to 400 m where LIW flows, and the deep layer below 400 m (Estournel et al., 2021). In this study, we will be focusing on the first two layers, as changes at greater depths are very slow over the 8-year period and barely detectable. The biogeochemical term of the oxygen budget is the sum of oxygen production due to gross primary production and nitrate uptake by phytoplankton, and of oxygen consumption through nitrification and community respiration. The physical term is divided into two components: the lateral and the vertical transports, which are both due to advection and mixing processes. The lateral transport represents the exchanges with the Ionian and Aegean seas. A negative lateral transport indicates a net export of oxygen from the considered layer of the Levantine Basin. The oxygen inventory, air-sea fluxes, biogeochemical fluxes, and lateral fluxes were calculated online while the vertical transport, defined as a net flux at the layer interface, was deduced from the other terms of the budget. The budget calculation is detailed in Text S1 in Supplement Material.

https://doi.org/10.5194/egusphere-2025-4028
Preprint. Discussion started: 16 September 2025

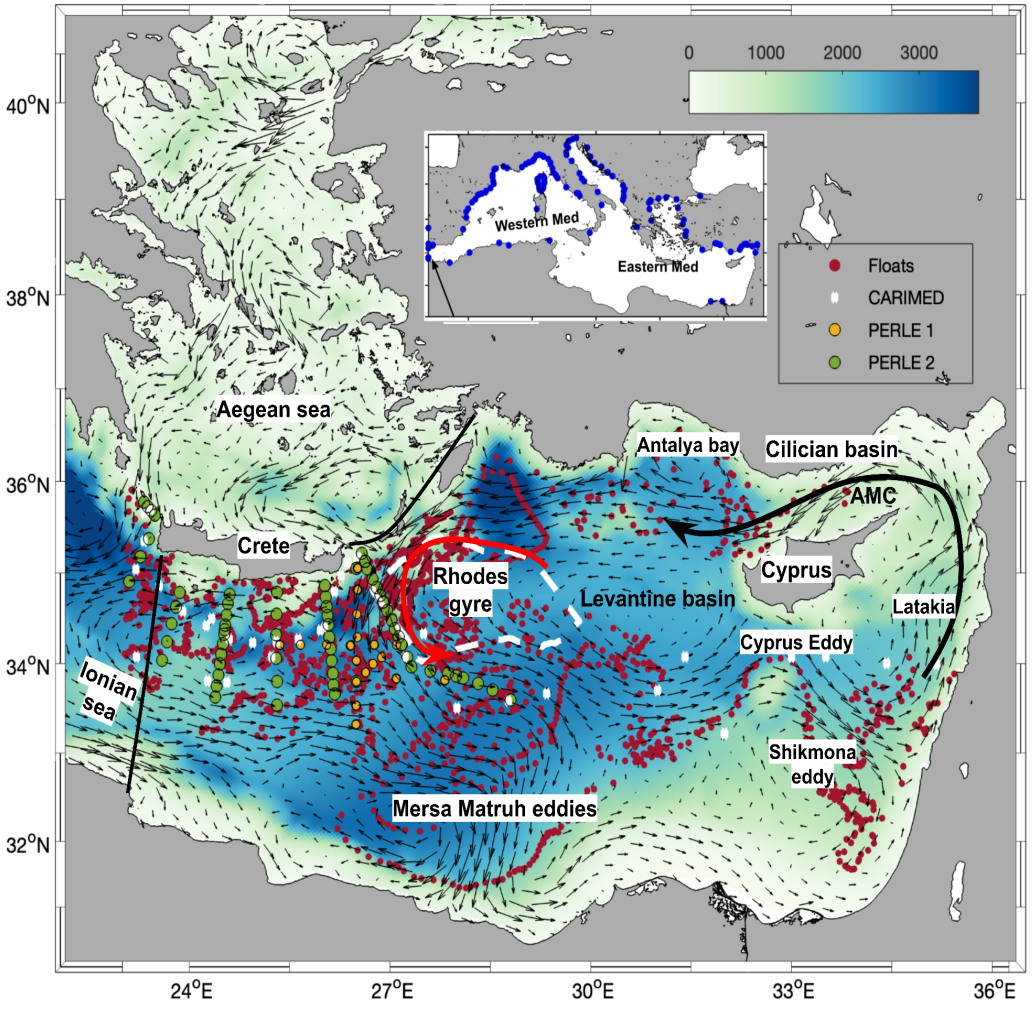

Figure 1: Model domain and bathymetry (m, background) in the Eastern Mediterranean. The arrows represent the simulated surface currents averaged over the study 7-year period (2013-2020), black thick lines delimit the basin for the budget calculation. Red, yellow, and green dots indicate BGC-Argo floats trajectories, PERLE-1, and PERLE-2 cruise stations, respectively, and white crosses CARIMED cruise stations, over the period from 2013 to 2021. Blue dots in the insert represent the river mouths.

2.2 Observations for model assessment

2.2.1. Argo float data

In order to assess the modeled temporal and spatial evolutions of the oxygen concentration, we use observations from Argo floats that were deployed in the Levantine Basin during the periods of 2013-2015 and 2015-2018. In particular,

https://doi.org/10.5194/egusphere-2025-4028
Preprint. Discussion started: 16 September 2025

we present comparisons with data provided by the two BGC-Argo floats 6901528 and 6901764 (151 and 173 vertical profiles, respectively). Temperature and salinity measurements were also extracted to calculate oxygen solubility. The oxygen data were downloaded from the Argo Global Data Assembly Center web portal accessible through the Coriolis database (http://www.coriolis.eu.org). Calibration of dissolved oxygen was performed at the deployment using in situ observations from 0 to 1000 m depth (Winkler titration). The calibration and the deployment strategy are detailed in (Thierry et al., 2021). The uncertainties of the measurements were estimated at ~ 2-10 µmol kg^{-1} depending on the sensor (Grégoire et al., 2021).

2.1.2 Cruise data and seawater measurements

During the period from October 2018 to March 2019, biogeochemical measurements were made in the context of PERLE (D'Ortenzio et al., 2021) in the Levantine Basin to describe the preconditioning and dispersion of the Levantine Intermediate Water (LIW) and to assess its role in structuring the phytoplankton ecosystem. In this study, we use data from two PERLE cruises: PERLE-1 (https://campagnes.flotteoceanographique.fr/campagnes/18000848/fr/) on board R/V l'Atalante in October 2018 and PERLE-2 on board R/V Pourquoi Pas? in February-March 2019 (Conan and Durrieu De Madron, 2019). PERLE-1 covers the period of the preconditioning of LIW formation during which an array of 25 CTD casts was set up. PERLE-2 covers the water formation period with 29 CTD oxygen casts (Fourrier, 2020). Stations of PERLE cruises are indicated in Fig. 1. Winkler analyses were performed onboard using photometric endpoint detection to adjust the SBE43 raw data. After sensor coefficient adjustment, the accuracy of the SBE43 sensor is estimated to be around 2 µmol kg^{-1}.

We also use the observations included in the CARIMED database, collected during four cruises that covered the farthest east and south of the basin: the Meteor M84/3 (Tanhua, 2013), HOTMIX (Arístegui, J., & UTM-CSIC. (2018). HOTMIX Cruise, RV Sarmiento de Gamboa [Data set]. UTM-CSIC. http://doi.org/10.20351/29SG20140427 SMASH), MEDSEA (Ziveri and Grelaud, 2015), and MSM72 (Hainbucher et al., 2020) cruises conducted during the period between 2011-2018. The seawater was collected using Niskin bottles from the surface to 4600 m of depth using an SBE43 oxygen sensor for the oxygen concentrations, followed by the modified Winkler potentiometric method (Martínez-Pérez et al., 2017). The spatial coverage of the datasets is shown in Fig. 1.

3 Results

3.1 Assessment of the model

An assessment of the hydrodynamic simulation was performed by Estournel et al. (2021), who showed the capacity of the model to reproduce the observed hydrology, as well as the surface and intermediate circulations. In Habib et al. (2023), the results of the biogeochemical model were evaluated in terms of spatial and temporal variabilities of chlorophyll, dissolved inorganic nutrients, and dissolved oxygen against satellite, cruise, and BGC-Argo float data. Here, we further assess the dissolved oxygen dynamics by providing supplementary comparisons with cruises, notably PERLE cruises, and Argo float data, as well as in situ measurements of metabolic rates.

https://doi.org/10.5194/egusphere-2025-4028
Preprint. Discussion started: 16 September 2025

3.1.1 Comparison with BGC-Argo float data

Figure 2 represents the temporal evolution of vertical profiles of oxygen from both the model and float observations over the first 500 m, as well as the surface oxygen concentration and oxygen solubility along the float's pathways that were selected for their broad spatio-temporal coverage, each capturing stratification and mixing periods at different locations (Fig. 2a). The observations and the model outputs exhibit the same seasonal variability (Fig. 2 d,e). During summer, both oxygen solubility and surface oxygen concentrations reach their minimum values. Oxygen solubility starts increasing following this period (Fig. 2d-e). Modeled and observed surface oxygen concentrations and solubility show correlation coefficients higher than 0.95 (p-value < 0.05) with a bias lower than 3 µmol O_2 kg^{-1}. The RMSD values (Root Mean Square Difference) are less than 5 µmol O_2 kg^{-1} for both floats and fall within the oxygen uncertainty interval associated with Argo float data.

The general observed features across the water column are respected by the model (Fig. 2b-c) with (i) a subsurface oxygen maximum formation in March/April when the water column restratifies, (ii) a deepening of oxygen maximum until December, followed by (iii) the erosion of the oxygen maximum and homogenization of the surface layer when vertical mixing intensifies, inducing a relatively deep mixed layer. The oxygen maximum in the subsurface layer is underestimated by ~5 µmol kg^{-1} by the model ($RMSD \simeq 8\ \mu mol\ kg^{-1}$) for the period while its depth is well located. Further deep, the concentration and the localization of the OML are well reproduced with a magnitude of 180 µmol kg^{-1} and depths between 380 and 500 m (Fig. 2b-c). Overall, the simulation reproduces correctly the spatial and temporal variability of the oxygen observed at the surface and in the water column.

https://doi.org/10.5194/egusphere-2025-4028
Preprint. Discussion started: 16 September 2025

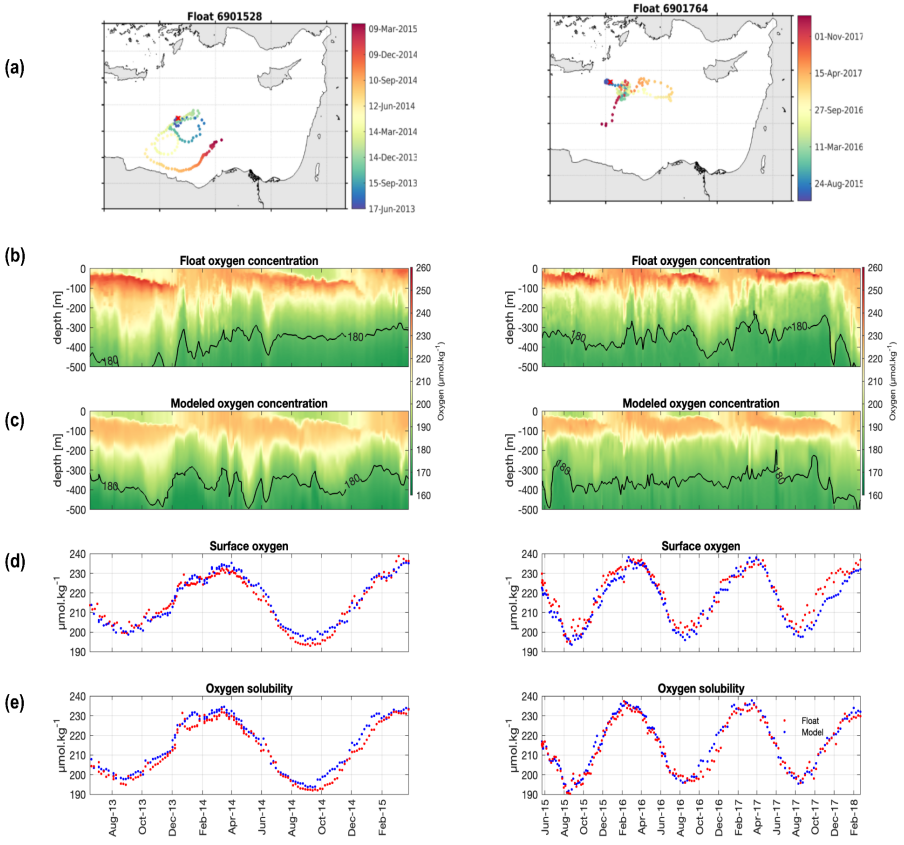

Figure 2: From top to bottom: (a) trajectory of the BGC-Argo floats with deployment position (red cross) and chronology in color; Hovmöller diagrams of oxygen concentration (µmol O_2 kg^{-1}) from (b) float data and (c) model outputs for the first 500 m; (d) surface oxygen concentration in the first 10 m (µmol O_2 kg^{-1}) and (e) oxygen solubility (µmol O_2 kg^{-1}), from the float data (red) and the model (blue).

3.1.2 Comparison with cruise data

Comparisons with data from PERLE-1, PERLE-2, and CARIMED cruises (Fig. S1) show that the model accurately reproduces the magnitude and variability of oxygen concentrations across the different water layers, consistent with observations from the floats comparison. The model and the data from PERLE1, PERLE2, and CARIMED significantly correlate (correlation coefficient higher than 0.95, p-value< 0.05). The model reproduces the intensity of the subsurface maximum reaching 230 µmol O_2 kg^{-1} during the PERLE 1 cruise in fall (Fig. S1a) contrary to its underestimation noted when comparing the model with the floats (Sect. 3.1.1). These differences between the floats and the cruise data and between the cruises (Fig. S2) could reflect differences in the sampling methods between each campaign of the dataset or mesoscale variability not correctly reproduced by the model.

https://doi.org/10.5194/egusphere-2025-4028
Preprint. Discussion started: 16 September 2025

The highest concentrations (230 µmol O_2 kg^{-1}) are located at the surface during the winter PERLE 2 cruise and CARIMED observations collected during the mixing period, for both model and observations (Fig. S1 b and d). Modeled dissolved oxygen concentrations below 100 m generally stand within the upper range of the observed values, except for the comparison with PERLE-2 observations, for which the model shows higher values all over the water column. The overestimation could be attributed to an overestimation of remineralization in this layer or vertical diffusion.

3.1.3 Comparison of process rates

Data on metabolic rates in the eastern Mediterranean Sea are scarce, and most available estimates are derived from observations made during stratified periods. Comparisons between model results averaged over periods from mid-June to mid-July and process rates measured near the surface and within the 145 m integrated layer in the core of an anticyclonic eddy in the eastern Levantine Basin during the BOUM cruise (Christaki et al., 2011) show that the modeled GPP, CR and NCP are in the upper range of the observational measurements. We also compared our model averages for May over the Levantine Basin with rates measured during the THRESHOLD cruises (Regaudie-de-Gioux et al., 2009) in the 5-110 m surface layer, and found values in the range of observations. In addition, model values integrated over the upper 100 m are consistent with those reported during the MINOS cruise (Moutin and Raimbault, 1996) conducted in the Levantine Basin between May and June. These comparisons can be found in Table 1.

Table 1: Comparison between averaged modeled and observation rates over the same period and along the same region. a: Lagaria et al., (2011), b: Christaki et al. (2011), c: Regaudie-de-Gioux et al. (2009), (d) Moutin and Raimbault (1996).

Process	Campaign	Region	Period	Layer	Observation	Model	Reference
GPP	BOUM	Core of an anticyclonic eddy in the eastern Levantine	mid-June to mid-July	Near the surface	0.12 ± 0.90 mmol O_2 m^{-3} day^{-1}	1.36 mmol O_2 m^{-3} day^{-1}	a
				Integrated 145 m	28-75 mmol O_2 m^{-2} day^{-1}	68 mmol O_2 m^{-2} day^{-1}	b
	THRESHOLD	Levantine Basin	May	5-110 m	0.16-2.93 mmol O_2 m^{-3} day^{-1}	1-8 mmol O_2 m^{-3} day^{-1}	c
	MINOS	Levantine Basin	May to June	Near the surface	0.59 ± 0.16 mmol O_2 m^{-3} day^{-1}	1.08 mmol O_2 m^{-3} day^{-1}	d
			May to June	Integrated 100m	37.9 ± 4.8 mmol O_2 m^{-2} day^{-1}	37 mmol O_2 m^{-2} day^{-1}	d
CR	BOUM	Core of an anticyclonic eddy in the		Near the surface	0.38 ± 0.92 mmol O_2 m^{-3} day^{-1}	1.28 mmol O_2 m^{-3} day^{-1}	a

https://doi.org/10.5194/egusphere-2025-4028
Preprint. Discussion started: 16 September 2025

		eastern Levantine	mid-June to mid-July	Integrated 145 m	39-58 mmol O_2 m^{-2} day^{-1}	68 mmol O_2 m^{-2} day^{-1}	b
	THRESHOLD	Levantine Basin	May	5-110 m	0.1-8.2 mmol O_2 m^{-3} day^{-1}	1-7 mmol O_2 m^{-3} day^{-1}	c
NCP	BOUM	Core of an anticyclonic eddy in the eastern Levantine	mid-June to mid-July	Near the surface	-0.26 ± 0.22 mmol O_2 m^{-3} day^{-1}	0.09 mmol O_2 m^{-3} day^{-1}	a
				Integrated 145 m	4 ± 15 mmol O_2 m^{-2} day^{-1}	0.9 mmol O_2 m^{-2} day^{-1}	b
	THRESHOLD	Levantine Basin	May	5-110 m	-6.4-8.2 mmol O_2 m^{-3} day^{-1}	0-2 mmol O_2 m^{-3} day^{-1}	c

3.2 Seasonal variability

3.2.1 Atmospheric forcing and vertical mixing

Figure 3 presents the mean annual cycle of the modeled air-sea heat flux, wind stress, mixed layer (ML) depth, and surface temperature, spatially averaged over the Levantine Sea from December 2013 to December 2020. During fall, the decrease in air temperature leads to significant sea surface heat loss, while intensified northern winds weaken stratification, gradually deepening the mixed layer (Fig. 3a-c). The sea surface temperature drops significantly (Fig. 3d). Heat loss events persist through winter, leading the surface temperature to reach a minimum of approximately 17°C and the mixed layer depth to gradually increase, peaking in January/February. The yearly maximum ML depth averaged spatially over the seven years is 108 ± 11 m (Table S1). In March/April, the sea surface starts gaining heat, and the surface temperature increases (Fig. 3a and 3d). The ML abruptly shallows but still exhibits large variations during early spring, in response to the events of continental cold winds. The frequency of intense wind events decreases in late spring/summer (Fig. 3b). Surface temperature reaches maximum values around 28 °C in August (Fig. 3d), and a thin ML settles until October. In the following, the annual cycle is divided into two successive periods based on the vertical mixing intensity. The first period is a mixing period, from October to March, and the second period is a stratified period, from April to September. The two periods were defined based on a mixed layer depth threshold of 25 m, following the criteria used by D'Ortenzio et al. (2008) and Houpert et al. (2015).

https://doi.org/10.5194/egusphere-2025-4028
Preprint. Discussion started: 16 September 2025

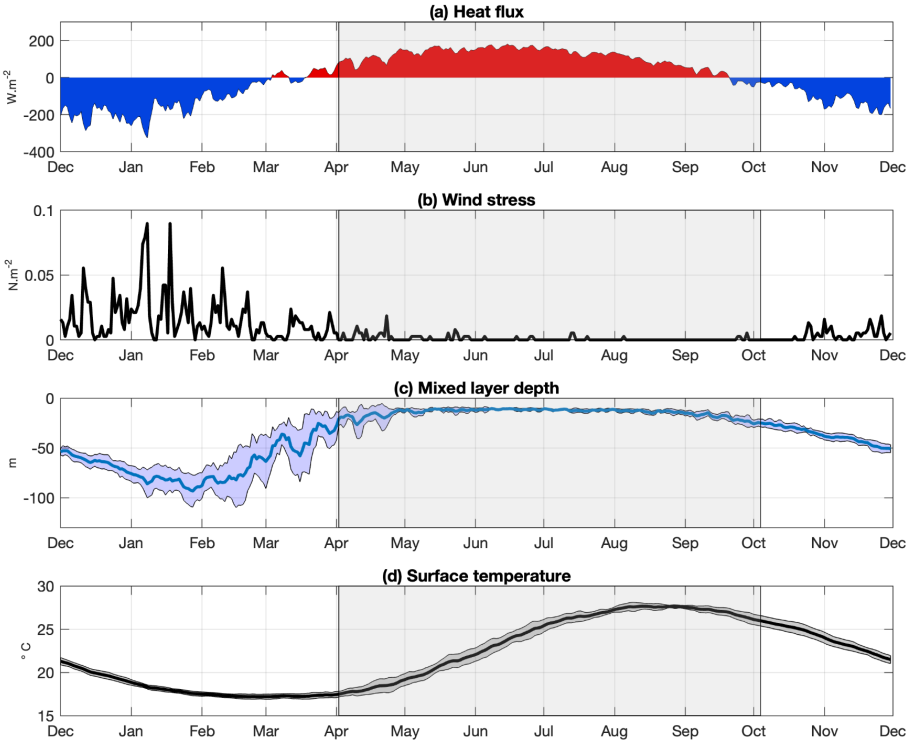

289

290 **Figure 3: Annual time series of modeled (a) air-sea heat fluxes (W m^{-2}), (b) wind stress (N m^{-2}), (c) mixed layer**
291 **depth (m), and (d) surface temperature (°C), averaged over the Levantine Sea and the period 2013-2020. In** (c)
292 **and (d), the solid line corresponds to the spatial mean, the shaded area to the standard deviation. The grey**
293 **shaded area represents the stratification period.**

294 **3.2.2 Oxygen fluxes**

295 The annual cycle of the 7-year averaged oxygen fluxes and inventory variation are described in Fig. 4 and 5, for the
296 surface and intermediate layers, respectively. The oxygen content in both layers increases during the mixing period
297 and gradually decreases during the stratified period with minimum values in November/December for the surface
298 layer and January for the intermediate layer (Fig. 4a and 5a). The vertical and net horizontal transports show a clear
299 seasonal variation, with the highest values of 50 mmol m^{-2} day^{-1} in winter in the surface layer and 50 mmol m^{-2} day^{-1}
300 and 40 mmol m^{-2} day^{-1} respectively in the intermediate layer (Fig. 4f and 5e). During the mixing period, mostly during
301 intense wind and mixing events (Fig. 3b-c), oxygen is exported from the surface layer towards the intermediate layer
302 (Fig. 4f), and then further down, from the intermediate towards the deep layer (Fig. 5e), with average export rates of
303 0.56 and 0.46 mol O_2 m^{-2} month^{-1}, respectively (Fig. S3b,d). During the stratified period, the downward export of O_2
304 towards the intermediate and deeper layers decreases by 75% and 40%, respectively (Fig. S3d). The oxygen horizontal

https://doi.org/10.5194/egusphere-2025-4028
Preprint. Discussion started: 16 September 2025

transport in the surface layer is characterized by a net inflow from the Ionian Sea and an outflow towards the Aegean Sea (Fig. 4g, S2b), with higher values during the mixing period compared to the stratified period (Ionian Sea: 1.3 vs 0.6 mol O_2 m^{-2} $month^{-1}$, and Aegean Sea: 0.9 vs 0.5 mol O2 m^{-2} $month^{-1}$, respectively, Fig. S3b). The horizontal exchanges in the intermediate layer show a less intense pattern with a stronger net inflow from the Ionian Sea (0.2 mol O_2 m^{-2} $month^{-1}$) and a stronger outflow towards the Aegean Sea (-0.4 O_2 mol m^{-2} $month^{-1}$, Fig. S3d and 5f) during the mixing period. The net oxygen flow in the surface layer remains directed from the Ionian and towards the Aegean across both periods, while the intermediate layer exhibits oxygen outflow toward both the Aegean and Ionian Seas (96% and 4% of the total horizontal export) during the stratified period, respectively (Fig. S3d).

The model results show that the Levantine Basin ecosystem in the surface layer produces dissolved oxygen from January to August, at higher rates between February and March, and consumes dissolved oxygen between September to December (Fig. 4d). Biogeochemical O_2 flux (NPC) accounts for a loss of 0.03 mol m^{-2} $month^{-1}$ over the mixing period (from October to April) and a gain of 0.06 mol m^{-2} $month^{-1}$ during the stratified period (Fig. S3a). The maximum magnitudes of biological production (> 2 mmol O_2 m^{-2} day^{-1}) are located near the surface during the periods of winter mixing and phytoplankton bloom, and then in the subsurface (Fig. 6f). The consumption is maximum in fall between 100 and 200 m depth, and during the mixing period below the mixed layer. During the stratified period, the relatively thick subsurface oxygen maximum (SOM) layer remains around 70 m depth, above the subsurface maximum biological production located at around 140 m depth close to the deep chlorophyll maximum (Fig. 6b, 6c, and 6f). This is in agreement with the findings of Di Biagio et al. (2022). As for the intermediate layer (150-400 m), it shows a loss of oxygen with values of biogeochemical flux above -10 mmol m^{-2} day^{-1} over the whole year (Fig. 5b).

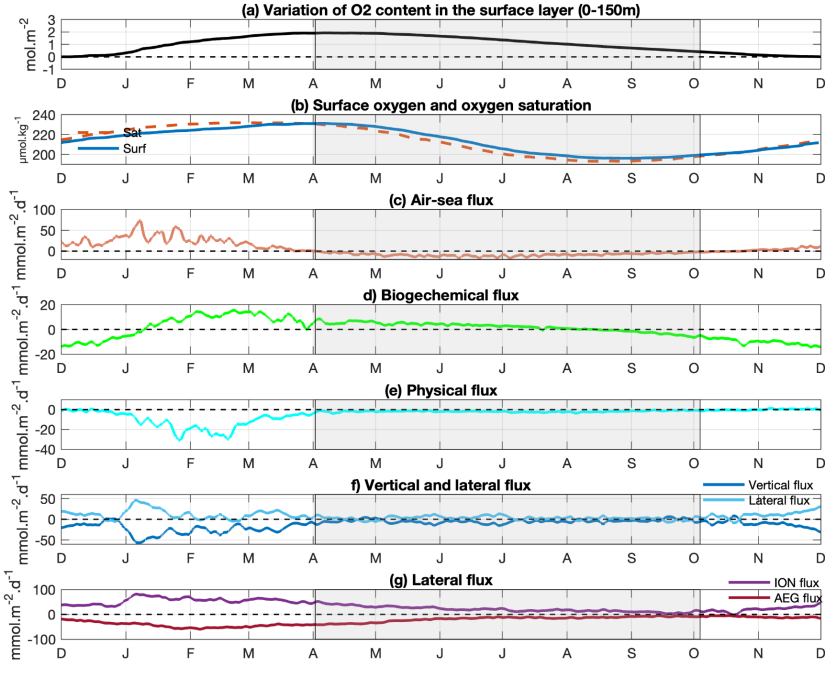

https://doi.org/10.5194/egusphere-2025-4028
Preprint. Discussion started: 16 September 2025

Figure 4: Oxygen concentration and budget of the 0-150 m layer of the Levantine Basin averaged over the period of study. (a) Variation of the dissolved oxygen inventory (mol m^{-2}) relative to initial conditions (Values are normalized to the starting time point), (b) surface oxygen concentration (blue) and oxygen solubility (orange) (µmol O_2 kg^{-1}), (c) air-sea flux (positive values correspond to downward fluxes, mmol O_2 m^{-2} day^{-1}), (d) biogeochemical flux (mmol O_2 m^{-2} day^{-1}), (e) sum of vertical (through the 150 m depth) and lateral (exchanges with the Ionian and Aegean Seas) transport fluxes (mmol O_2 m^{-2} day^{-1}), (f) vertical (light blue) and lateral (dark blue) fluxes (mmol O_2 m^{-2} day^{-1}), (g) lateral fluxes at the boundary with the Ionian (purple) and Aegean (red) Seas (mmol O_2 m^{-2} day^{-1}). Horizontal transport fluxes are scaled to the area of the Levantine basin for comparison with the other budget terms.The grey shaded area represents the stratification period.

The air-sea flux displays a seasonal pattern (Fig. 4b). During the October-April mixing period, the Levantine Basin, undersaturated in oxygen compared to the atmosphere, is a sink of atmospheric oxygen. Oxygen solubility has increased (Fig. 4b) with the decrease in surface temperature (Fig. 3d) since September. In parallel, the gradual deepening of the mixed layer favors an increase in the surface oxygen concentration, through the mixing of surface O_2 poorer waters with subsurface O_2-rich waters (Fig. 6c), which remains lower than the oxygen at saturation level. The air-sea flux, particularly strong in winter when the wind is intense, reaches maximal values around 70 mmol m^{-2} day^{-1} beginning of January (Fig. 4c). The air-sea flux averaged during the mixing period amounts to 0.50 mol O_2 m^{-2} $month^{-1}$ (Fig. S3a). At the onset of the stratified period (April - May), surface oxygen concentration reaches 230 µmol kg^{-1} (Fig. 4b), slightly exceeding saturation levels due to biological oxygen production in the surface layer (Sect. 3.2.4). As a result, the Levantine Basin becomes a source of oxygen for the atmosphere (Fig. 4c). During the rest of the stratified period, the surface oxygen concentration continues to present values higher than the oxygen solubility, leading to continuous outgassing of O_2. We estimate a mean net release of 0.26 mol O_2 m^{-2} $month^{-1}$ of oxygen to the atmosphere over the whole stratified period (Fig. S3a).

https://doi.org/10.5194/egusphere-2025-4028
Preprint. Discussion started: 16 September 2025

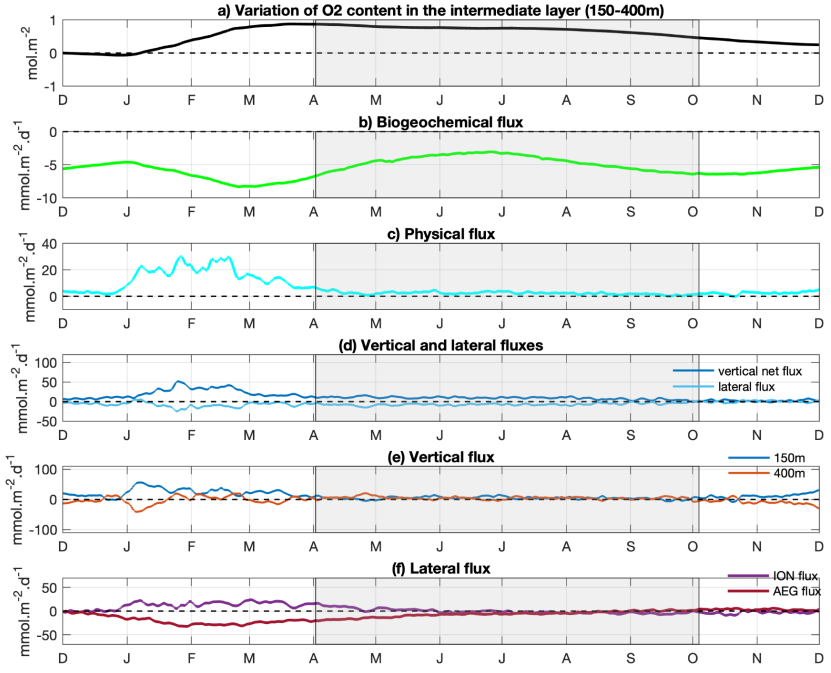

Figure 5: Mean annual cycle of (a) variation of the dissolved oxygen inventory (mol m^{-2}) relative to initial conditions (Values are normalized to the starting time point), and the different oxygen fluxes (mmol m^{-2} day^{-1}): (b) biogeochemical flux, (c) total vertical and horizontal transport, (d) vertical (downward) flux (light blue) and lateral flux (dark blue), (e) the vertical fluxes at 150 and 400m and (f) the lateral Ionian (purple) and Aegean (red) fluxes, in the intermediate layer (150-400 m) and averaged over the Levantine Basin. The grey shaded area represents the stratification period.

https://doi.org/10.5194/egusphere-2025-4028
Preprint. Discussion started: 16 September 2025

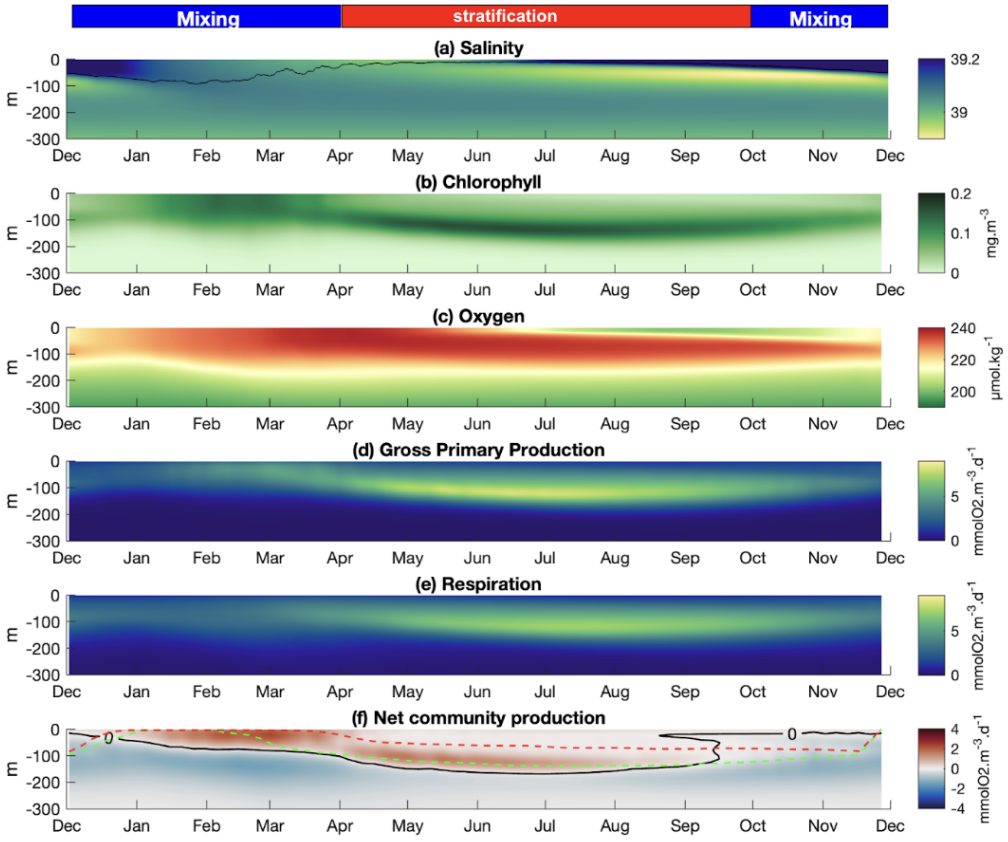

Figure 6: Hovmöller diagrams of (a) salinity, (b) chlorophyll (mg m^{-3}), (c) dissolved oxygen concentration (µmol kg^{-1}), (d) gross primary production (mmol m^{-2} day^{-1}), (e) community respiration (mmol m^{-2} day^{-1}), and (f) net community production (mmol m^{-2} day^{-1}), averaged over the Levantine Basin, from December 2013 to May 2021. The black line in (a) indicates the mixed layer depth.

3.3. Interannual variability

We investigated correlations between processes operating at the annual scale and seasonal fluxes, identifying winter as the most influential period. In the following section, we therefore focus our analysis on winter. For the purposes of this study, the year is defined as running from December to the following December.

3.3.1 Atmospheric forcing and vertical mixing

Winter (December-January-February) heat loss exceeded the seasonal mean value of 152 W m^{-2} for years 2014-15, 2016-17, 2018-19, and 2019-20 (Fig. 7a, Table S1). In contrast, wind stress does not show consistent interseasonal variability, with peak values around 0.2 N m^{-2} occurring each year (Fig. 7b). The ML depth presents interannual variability mostly associated with heat loss fluxes (Fig. 7a and 7c), with higher values than the averaged one of 108

https://doi.org/10.5194/egusphere-2025-4028
Preprint. Discussion started: 16 September 2025

m during the winters 2014-15, 2016-17, and 2018-19 (Table S1). Based on the mean winter heat flux, and mean and maximum ML, the years were classified as mild and cold winter years: years with both winter heat loss and maximum ML above the seven-year means, i.e. 2014-15, 2016-17 and 2018-19, are considered cold winter years while, 2013-14, 2015-16, 2017-18 and 2020-21 are considered mild years.

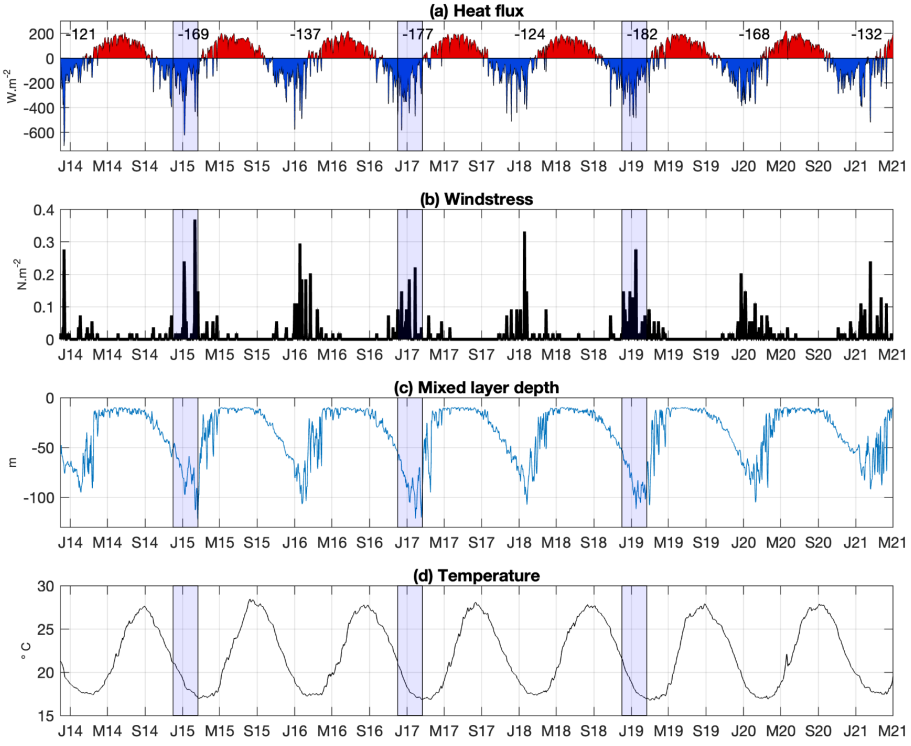

Figure 7: Time series of modeled (a) air-sea heat fluxes (W m^{-2}), (b) wind stress (N m^{-2}), and (c) mixed layer depth (m) averaged over the Levantine Basin. The mean winter (December-January-February) heat loss is indicated in (a). The blue shaded area represents the winter of the cold winter years.

3.3.2 Dissolved oxygen fluxes in the surface and intermediate layers

All years display qualitatively similar seasonal oxygen cycles in the surface layer (Fig. 8). However, colder years (2014–15, 2016–17, 2018–19) exhibit the highest fluxes and greater inventory variations. In winter, oxygen inventory changes exceed 2 mol O_2 m^{-2} (Fig. 8a). During phytoplankton blooms in these cold winters, biogeochemical fluxes surpass 20 mmol m^{-2} day^{-1} (Fig. 8d). Lateral and vertical transports of dissolved oxygen at the surface layer boundaries show peaks of inflow from the Ionian Sea, outflow toward the Aegean Sea, and downward export to the intermediate layer, exceeding 100, 75, and 100 mmol m^{-2} day^{-1}, respectively (Fig. 8f–g). Air-sea oxygen fluxes also exceed 150 mmol m^{-2} day^{-1} (Fig. 8c).

https://doi.org/10.5194/egusphere-2025-4028
Preprint. Discussion started: 16 September 2025

In the intermediate layer, cold winter years also present the highest O_2 winter fluxes and oxygen inventory variation compared to mild winter years (Fig. 9). Biogeochemical flux exhibits pronounced negative peaks exceeding 10 mmol m^{-2} day^{-1} during cold winter years (Fig. 9b). While these negative fluxes are not significantly stronger than in warm years, the subsequent positive fluxes are markedly enhanced following cold winters (less observed during 2016-17). Physical fluxes also are marked by a higher magnitude (Fig. 9c-f). As found in the upper layer, higher lateral and vertical oxygen exchanges occur during the cold winters. Along with the seasonal internal variation, an increasing trend in the inventory is visible from 2013-14 to 2018-19, followed by a decreasing trend until the end of the study period (Fig. 9a).

Oxygen fluxes are partly linked to winter heat loss (W-HL). There is a strong correlation between winter oxygen downward export from the surface layer and mean W-HL ($R = 0.76$, p-value < 0.05, Fig. S4). Cold years also show high NCP (Net Community Production: gross primary production (GPP) minus community respiration (CR)) flux, with a significant correlation between mean W-HL and annual NCP ($R = 0.91$, p-value < 0.05, Fig. S4). When W-HL drops below 135 W m^{-2}, the system shifts from autotrophic to heterotrophic. In the intermediate layer, annual oxygen consumption remains relatively stable but is still significantly correlated with W-HL ($R = 0.94$, p-value < 0.05). Air-sea oxygen fluxes also show strong correlations with W-HL ($R = 0.92$ annually, $R = 0.93$ in winter, p-value < 0.05). While lateral fluxes increase during cold years, only exchanges with the Aegean Sea show a significant correlation with W-HL ($R = 0.74$ in the surface layer, $R = 0.82$ in the intermediate layer). The correlation with the Ionian Sea is weaker and not statistically significant ($R = 0.69$, p-value < 0.08).

https://doi.org/10.5194/egusphere-2025-4028
Preprint. Discussion started: 16 September 2025

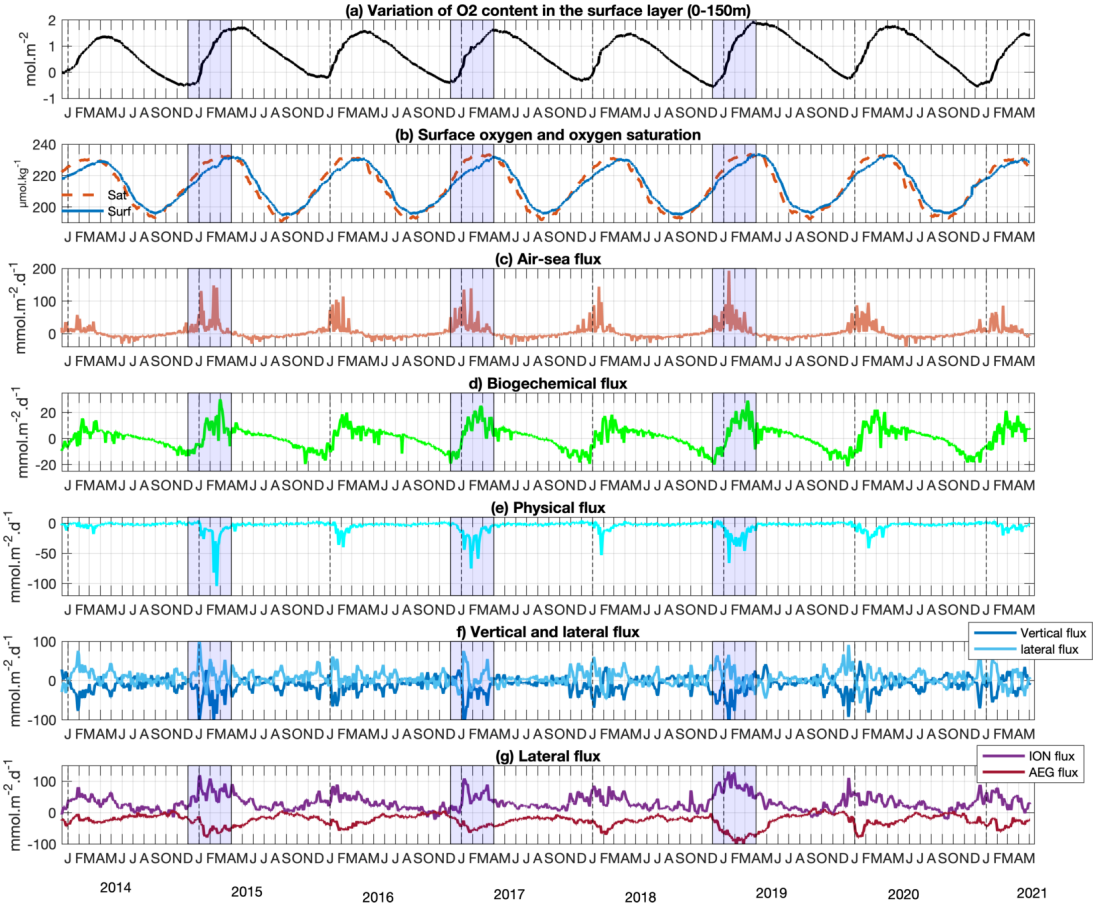

Figure 8: Time series of oxygen concentration and budget of the 0-150 m layer of the Levantine Basin. (a) Variation of the dissolved oxygen inventory (mol m^{-2}) relative to initial conditions (Values are normalized to the starting time point), (b) surface oxygen concentration (blue) and oxygen saturation (orange) (µmol O_2 kg^{-1}), (c) air to sea flux (mmol O_2 m^{-2} day^{-1}), (d) biogeochemical flux (mmol O_2 m^{-2} day^{-1}), (e) sum of vertical (through the 150 m depth) and lateral (exchanges with the Ionian and Aegean Seas) transport fluxes (mmol O_2 m^{-2} day^{-1}), (f) vertical (light blue), lateral (dark blue) flux (mmol O_2 m^{-2} day^{-1}), (g) detailed lateral flux at the boundary with the Ionian (purple) and Aegean (red) seas (mmol O_2 m^{-2} day^{-1}). Horizontal transport fluxes are scaled to the area of the Levantine Basin for comparison with the other budget terms. The blue shaded area represents the winter of the cold winter years.

https://doi.org/10.5194/egusphere-2025-4028
Preprint. Discussion started: 16 September 2025

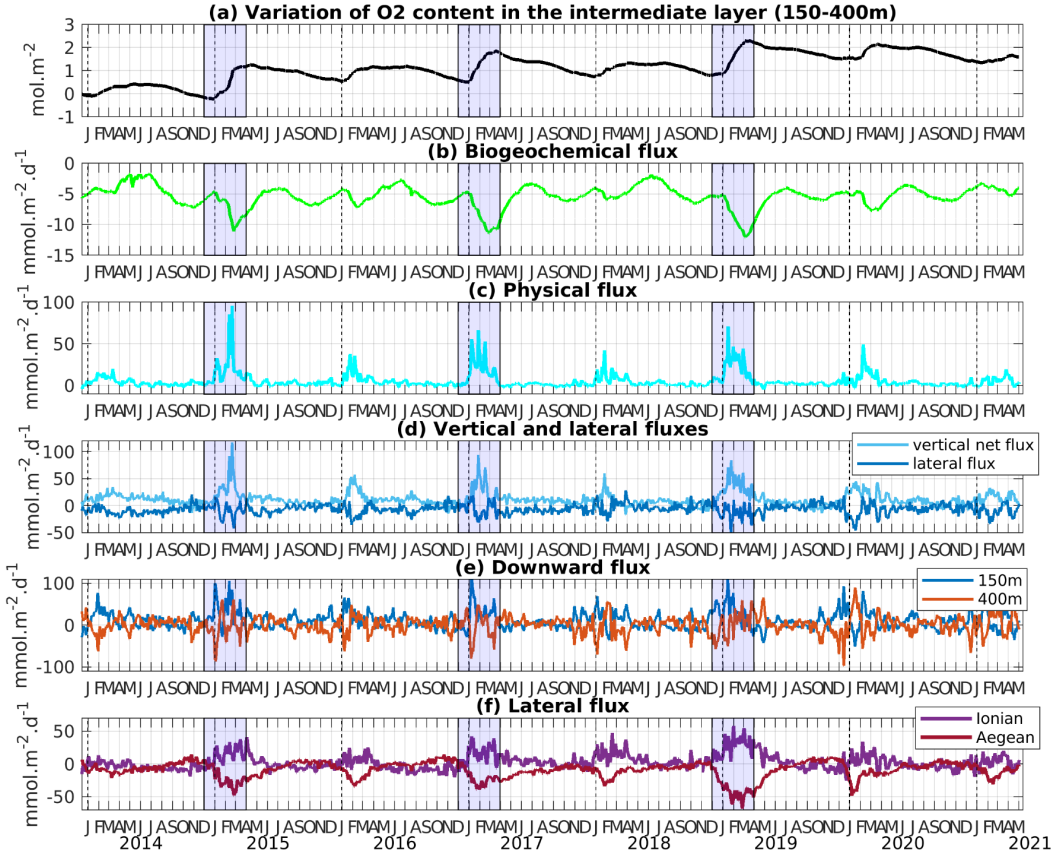

Figure 9: Time series of (a) variation of the dissolved oxygen inventory (mol m^{-2}), (b) biogeochemical flux, (c) total vertical and horizontal transport, (d) vertical (light blue) and lateral flux (dark blue), and (g) lateral fluxes from Ionian (purple) and Aegean (red) sea, in the intermediate layer (150-400 m) and averaged over the Levantine Basin. The flux unit is mmol m^{-2} day^{-1}. The blue shaded area represents the winter of the cold winter years.

3.4 Annual oxygen budget in the surface and intermediate layers

On an annual basis and on average over the seven studied years (Fig. 10), the surface layer gains oxygen through air-sea exchange. Additionally, oxygen is transported from the Ionian Sea to the Aegean Sea through both surface and intermediate layers. A fraction of this oxygen is exported to intermediate depths, where it is partially consumed before the remainder reaches the Aegean (Fig. 10). The surface ecosystem of the basin appears to be generally productive in oxygen. The net biogeochemical flux is one order of magnitude smaller than transport and air-sea flux, changing sign depending on the considered year, with a strong interannual variability. On average, the intermediate layer loses oxygen due to biogeochemical consumption but gains it through net transport (Fig. 10). The physical supply of oxygen

https://doi.org/10.5194/egusphere-2025-4028
Preprint. Discussion started: 16 September 2025

comes from both downward inflow from the surface layer and lateral inflow from the Ionian Sea, while part of the oxygen is exported toward the Aegean Sea (Fig. 10).

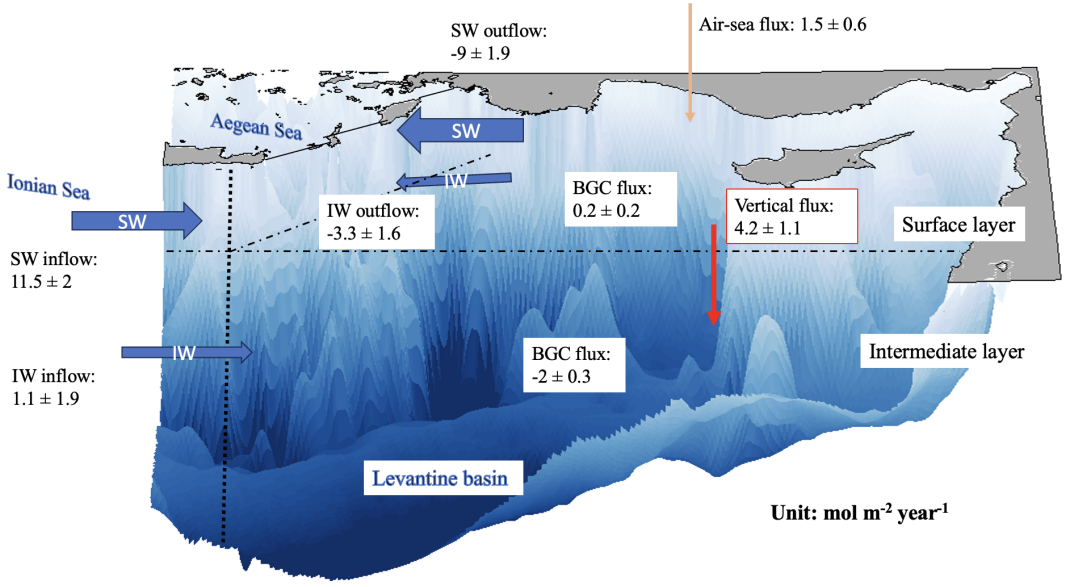

Figure 10: Schematic showing the terms of the mean annual oxygen budget (in mol O_2 m^{-2} yr^{-1}) for the Levantine Basin over the period from December 2013 to November 2020. The terms of the budget are estimated for the upper layer (surface-150 m), and the intermediate layer (150-400 m). SW: surface layer, IW: intermediate layer. Arrow thickness is proportional to the intensity of the flow.

3.5 Spatial variability of oxygen fluxes in the Levantine Basin

At the annual scale, the whole Levantine Basin appears as an atmospheric sink for oxygen, except in the coastal area influenced by the Nile River (Fig. 11a). The highest uptake rates in the offshore region are located in the Rhodes Gyre area, covering 5% of the surface of the Levantine Basin, and contributing 14% of the annual atmospheric oxygen intake. Other regions characterized by higher uptake rates are located in the North, in the Antalya Bay and the Cilician basin. The annual air-sea flux is also spatially mostly controlled by the winter air-sea O_2 flux (not shown). The annual anomalies show that the cold years (2014-15, 2016-17 and 2018-19) absorb more atmospheric oxygen in the whole sea (Table S2), and especially in the Rhodes Gyre (Fig. S7). In this area of intermediate water formation, the supply of cold and oxygen-poorer water from the intermediate layer towards the surface during the winter mixing period is more pronounced than in surrounding areas. Thus, the negative temperature anomaly, as well as the negative oxygen anomaly, enhanced the undersaturation in this area that shows maximum values varying between 2 and 5 % (with higher values during cold winter years). In contrast to the entire basin, where oxygen is exported from surface to intermediate layers, the model indicates that the Rhodes Gyre displayed an inverse pattern, with oxygen transported upward from intermediate depths to the surface, balanced by a lateral export. This lateral transfer is strong in winter and takes place notably through the dispersal of LIW by subduction (Estournel et al., 2021). The model results also show a spatial heterogeneity of the balance between GPP and CR, averaged along the period of study in the surface

https://doi.org/10.5194/egusphere-2025-4028
Preprint. Discussion started: 16 September 2025

450 layer (surface-150 m) (Fig. 11b). Positive NCP values are found in a central area including the cyclonic Rhodes and
451 cyclonic gyres (West Cyprus gyres,...), and the coastal areas influenced by rivers. In particular, the Rhodes Gyre
452 contributes to 41% of the annual biological oxygen production in the surface layer of the whole basin. NCP is negative
453 in the along-slope circulation, and in the anticyclonic Mersa-Matruh Eddies and Shikmona Eddy. It follows the same
454 spatial pattern throughout all the years with a more accentuated production in the cyclonic gyres during cold years
455 compared to the mild years (Fig. S6).

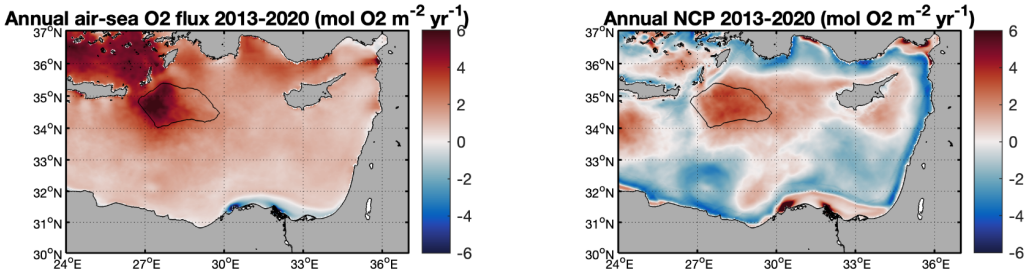

456

457 **Figure 11: Modeled annual air-sea oxygen flux and net community production (mol O_2 m^{-2} yr^{-1}) in the surface**
458 **layer (0-150 m) for the period from December 2013 to December 2020. The black line delimits the Rhodes gyre.**

459 **4 Discussion**

460 In the present study, we have used a 3D coupled physical-biogeochemical model to investigate the dynamics of oxygen
461 in the Levantine Basin. The physical and biogeochemical parts of the coupled model were previously validated by
462 Estournel et al. (2021) and Habib et al. (2023), respectively. Here we have further compared our results on the oxygen
463 cycle with two types of *in situ* data: high-resolution BGC-Argo data and data from research cruises. The major
464 limitation highlighted by these comparisons is the representation of the subsurface oxygen maximum layer. The
465 observed heterogeneity of this layer, with a maximum concentration in the upper part and then a progressive decrease
466 of its value further deeper, is not well reproduced in the model. The increase of the maximum value during the summer
467 period, shown in the BGC-Argo data, could be attributed to production or respiration processes, underestimated or
468 overestimated, respectively, in the model. This discrepancy could also be explained by physical processes with a
469 misrepresentation of the thickness of the subsurface oxygen maximum layer in the model. In that case, a finer vertical
470 resolution at those depths or an improvement of the vertical advection scheme, avoiding possible spurious numerical
471 mixing, as proposed by Garinet et al. (2024), could be tested in future works to reduce the vertical diffusivity. Despite
472 this limitation, the seasonal variations of oxygen solubility and concentration align with previous observational studies
473 (Kress and Herut, 2001; Schlitzer et al., 1991) and we used the model to estimate the contribution of various
474 processes—air-sea flux, physical dynamics, and biogeochemical processes—to oxygen dynamics and the overall
475 budget.

476 The model shows a net annual weak biological production of oxygen in the surface layer of the Levantine Basin,
477 primarily due to the sea's oligotrophic nature, which is more pronounced in the southeastern regions of the Levantine
478 Basin (D'Ortenzio, 2009; Lavigne et al., 2015). This oligotrophy is attributed to an anti-estuarine circulation
479 characterized by an eastward inflow of surface nutrient-depleted waters and an outflow of intermediate nutrient-rich

https://doi.org/10.5194/egusphere-2025-4028
Preprint. Discussion started: 16 September 2025

waters resulting from the water formation (Robinson and Golnaraghi, 1993). Interannual variability is observed here, with the sea being heterotrophic during warm winter years (2014 and 2018 here), as detected by Mayot et al. (2016) using satellite ocean color data. By considering both surface and intermediate layers, the Levantine Sea appears as a heterotrophic system in the model results. This aligns with the review by Siokou-Frangou et al. (2010) and the study by Christaki et al. (2011), depicting a large temporal and spatial heterogeneity in the trophic status of the oligotrophic Levantine Basin. The planktonic ecosystem in the Levantine Basin is strongly regulated by the basin's heterotrophic component. Siokou-Frangou et al. (2002) observed an increase in the heterotrophic/autotrophic biomass ratio with higher values more frequently found in the oligotrophic regions and during the stratified period. This pattern aligns with the spatial trend reported by Christaki et al. (2002), who depicted a longitudinal increase in this ratio from the Balearic Sea to the eastern Levantine Sea. Despite this heterotrophic system, highly dynamic mesoscale physical structures favoring deep vertical mixing, and in particular nutrient upwelling, determine the trophic gradient of the Levantine Basin (Siokou-Frangou et al., 2010), varying from marked recycled production to new production systems (Legendre and Rassoulzadegan, 1995). This variability was also detected in nutrient concentrations from different parts of the Levantine Basin. A shallow nutricline, coupled with an upward nutrient flux, was found in cyclonic systems, whereas the opposite effect occurred in anticyclonic systems (Salihoğlu et al., 1990). This pattern was also reflected in the spatial distribution of chlorophyll. Our model results show the high contribution of the Rhodes Gyre to the annual oxygen biological production in the surface layer of the whole Levantine Basin area (around 41%). In the intermediate layer, biogeochemical fluxes exhibit little variation between mixing and stratification periods, especially during cold years, consistent with the findings of Roether and Well (2001) and Klein et al., (2003).

The model indicates that the Levantine Basin absorbs atmospheric oxygen from November to April, while releasing it during the rest of the year. This is in line with the studies of Schlitzer et al. (1991), Kress and Herut, (2001), and Di Biagio et al. (2022). The whole Levantine Basin, except the river-influenced areas (Nile river), shows an annual atmospheric uptake for all studied years (1.5 ± 0.6 mol O_2 m^{-2} yr^{-1}), with higher values during cold winter years. The uptake is enhanced in intermediate water formation areas, in particular in the Rhodes Gyre, where the undersaturation is increased during the winter period, when poorer O_2 water masses are mixed with surface waters, in agreement with what was previously observed and modeled in other water formation areas (Copin-Montégut and Bégovic, 2002; Coppola et al., 2017, 2018; Di Biagio et al., 2022; Fourrier et al., 2022; Körtzinger et al., 2004, 2008; Ulses et al., 2021; Wolf et al., 2018). The Rhodes Gyre shows a comparable winter uptake rate (20.3 ± 7.4 mol O_2 m^{-2} yr^{-1}) as other water formation areas such as the Labrador Sea and Gulf of Lion (ranging between 11 and 37 mol m^{-2}; Copin-Montégut & Bégovic, 2002; Coppola et al., 2017, 2018; Körtzinger et al., 2008; Ulses et al., 2021; Wolf et al., 2018). As a matter of comparison, the 7-year averaged oxygen uptake estimated here for the whole Levantine Basin, characterized by relatively low solubility compared to the rest of the Mediterranean (Mavropoulou et al., 2020, Di Biagio et al., 2022), represents 64% of the oxygen uptake by the NW Mediterranean deep convection estimated for the cold year 2012-13 with the same coupled model (Ulses et al., 2021).

Regarding the oxygen vertical transport in the whole Levantine Basin, the weak transfer from the deep layer into the intermediate layer found in our results is consistent with the general scheme of circulation or oxygen cycle shown in previous studies (Mavropoulou et al., 2020; Powley et al., 2016; Roether and Schlitzer, 1991; Tanhua et al., 2013) describing a gradual upwelling of deep water originating from the Adriatic Sea or Aegean Sea. While a downward export of oxygen from the surface layer to the intermediate layer is simulated at the scale of the whole basin, the Rhodes Gyre exhibits an opposite pattern, with oxygen being transported upward from the intermediate layers to the

https://doi.org/10.5194/egusphere-2025-4028
Preprint. Discussion started: 16 September 2025

surface. This input in the surface layer is balanced by a lateral export, particularly strong in winter, which takes place notably through the dispersal by subduction of the newly formed LIW as reported by Malanotte-Rizzoli et al. (2003) for January 1995 during the POEM cruise.

Our results on lateral oxygen exchanges are also in agreement with previous studies describing the general circulation in the eastern Mediterranean Sea. Regarding the exchanges with the Aegean Sea, a net outflow of LSW and LIW by the Asia Minor Current through the Cretan Straits was documented in several observational and modeling studies (Estournel et al., 2021; Millot and Taupier-Letage, 2005; Theocharis et al., 1993; Velaoras et al., 2014; Zodiatis, 1993). As for the exchanges with the Ionian Sea, the general cyclonic circulation displays in the surface and intermediate layers an eastward inflow along the Libyan-Egyptian coast (Estournel et al., 2021). South of Crete, the flux reverses seasonally with an inflow from the Ionian in winter and an outflow in summer (Estournel et al., 2021).

5 Conclusion

The study period was marked by contrasted atmospheric and hydrodynamic winter conditions. The confrontation of the model results with cruise and BGC-Argo float observations shows the capacity of the model to capture the general seasonal and spatial dissolved oxygen variability and the main oxygen features in the basin. These in situ observations, particularly from BGC-Argo floats and ship-based measurements, were essential in constraining and validating the simulations, without which the model outputs would not have reached their current level of reliability. The following conclusions can be drawn:

- The model results indicate a clear seasonal cycle for the oxygen air-sea flux. During winter, with the decrease in temperature, the increase in heat losses and mixing events, the surface layer is undersaturated in oxygen and thus absorbs atmospheric oxygen at the surface. The undersaturation averaged over the whole basin reaches 2 % during winter. During the stratified period, primary production in the surface layer leads to oxygen oversaturation and subsequent outgassing, with a maximum oversaturation of 0.6% observed in summer.

- The Levantine Basin acts as a sink for the atmospheric oxygen at an annual scale, capturing 1.5 ± 0.6 mol O_2 m^{-2} yr^{-1} of oxygen. Most of the oxygen uptake occurs during winter when it accounts for 10.7 ± 2.8 mol O_2 m^{-2} yr^{-1}. The Rhodes Gyre absorbs atmospheric oxygen at a 2-fold higher rate than the whole Levantine Basin.

- Our budget shows that the surface layer of the Levantine Basin is a source of dissolved oxygen for the intermediate depths, with winter vertical export of oxygen influenced by the winter heat loss intensity. Regarding the exchanges with the surrounding seas, we found that oxygen is laterally transported from the Ionian Sea into the basin, and from the basin towards the Aegean Sea. The lateral annual oxygen outflow to the Aegean is strongly enhanced by the heat loss intensity with exports 1.5 and 2.4 times higher during cold years in the surface and intermediate layer, respectively, compared to mild years.

- The Levantine Basin is found to act as a weak autotrophic ecosystem on an annual level, with a net community production in the surface layer alternating between auto- and heterotrophic status influenced by the magnitude of the winter heat loss. In deeper depths, respiration and nitrification resulted in an oxygen

https://doi.org/10.5194/egusphere-2025-4028
Preprint. Discussion started: 16 September 2025

consumption of 2.0 ± 0.3 mol O_2 m^{-2} yr^{-1}. Spatially, the Rhodes Gyre appears to be a major oxygen reservoir across the basin, contributing 41% of the oxygen production of the whole surface layer.

This work represents a first step in our modeling of the dissolved oxygen dynamics in the Levantine Basin. Further investigations on the role of the various cyclonic and anticyclonic eddies will be conducted in the future. Besides, several studies suggest a decadal variability of dissolved oxygen across the whole water column linked to the dense water formations in the south Adriatic and Aegean seas and to the general eastern Mediterranean circulation, notably the reversal of the North Ionian Gyre (Ozer et al., 2020, 2022). A time-extended simulation of the coupled model, in addition to the implementation of a finer vertical resolution at key depths, could contribute to examining this longer variability in the Levantine Basin and the connections between the sub-basins of the eastern Mediterranean.

In memoriam

The authors wish to pay tribute to the memory of Pascal Conan, who passed away on August 5, 2025. He made insightful contributions and was unwaveringly dedicated to biogeochemical oceanography. We will greatly miss him both professionally and personally.

Code availability

The SYMPHONIE model and the MATLAB codes used to process the model outputs are available from the authors on request.

Data availability

Data used to validate the model are available on different websites specified in the main text of the paper. These data and the model outputs are also available from the authors on request.

Author contributions

CU, CE, and JH conceptualized the study. CE and PM ran the SYMPHONIE model. PM added the budget calculation to the coupled model. CU and JH calibrated and ran the coupled physical–biogeochemical model. CE validated the physical model, JH the biogeochemical model. Observational data were provided by PC, MPP, MaF, LC, CWR, DL and TM. Funding acquisition was done by MiF, CU and CE. JH, CU, and CE wrote the initial version of paper. All authors contributed to the revision of the paper and approved the submitted version.

Acknowledgements

This study is a contribution to the MerMex (Marine Ecosystem Response in the Mediterranean Experiment) project of the MISTRALS international program. The numerical simulations were performed using the SYMPHONIE model, developed by the Community Code SIROCCO (https://sirocco.obs-mip.fr/) coordinated by the Research Infrastructure ILICO (CNRS-IFREMER) dedicated to coastal ocean observations (https://www.ir-ilico.fr/?PagePrincipale, last access: 16 June 2025), and computed on the cluster of LAERO/OMP and HPC resources from CALMIP grants (P1331). We acknowledge the scientists and crews of the Flotte océanographique française (https://www.flotteoceanographique.fr/), who contributed to the cruises carried out in the framework of the PERLE

https://doi.org/10.5194/egusphere-2025-4028
Preprint. Discussion started: 16 September 2025

project. We thank Franck Dumas, chief scientist of the PERLE 1 campaign, for his role in organizing and leading the cruise. The authors would like to acknowledge the National Council for Scientific Research of Lebanon (CNRS-L), Campus France, the University of Toulouse, and LEGOS for granting a doctoral fellowship to Joelle Habib. We thank Marta Álvarez (IEO, La Coruña) and collaborators for making the CARIMED database available to us.

Financial support

This research has been supported by the international programme MISTRALS (Marine Ecosystem Response in the Mediterranean Experiment – MerMex; https://www.odatis-ocean.fr/activites/activites-liees-au-pole/chantiers/mistrals, last access: 18 August 2025). The numerical simulations were performed with the SYMPHONIE model developed by the Community Code SIROCCO (https://sirocco.obs-mip.fr/) and coordinated by the Research Infrastructure ILICO (CNRS–IFREMER; https://www.ir-ilico.fr/?PagePrincipale, last access: 18 August 2025), with computational resources provided by the cluster of LAERO/OMP and CALMIP grants (P1331). The study also received support from the National Council for Scientific Research of Lebanon (CNRS-L), Campus France, the University of Toulouse, and LEGOS through a doctoral fellowship granted to Joelle Habib.

References

Álvarez, M., Velo, A., Tanhua, T., Key, R., and van Heuven, S.: CARBON, TRACER AND ANCILLARY DATA IN THE MEDSEA, CARIMED: AN INTERNALLY CONSISTENT DATA PRODUCT FOR THE MEDITERRANEAN SEA., 2019.

Arístegui, J., & UTM-CSIC. HOTMIX Cruise, RV Sarmiento de Gamboa [Data set]. UTM-CSIC. https://doi.org/10.20351/29SG20140427, 2018.

Auger, P. A., Diaz, F., Ulses, C., Estournel, C., Neveux, J., Joux, F., Pujo-Pay, M., and Naudin, J. J.: Functioning of the planktonic ecosystem on the Gulf of Lions shelf (NW Mediterranean) during spring and its impact on the carbon deposition: a field data and 3-D modelling combined approach, Biogeosciences, 8, 3231–3261, https://doi.org/10.5194/bg-8-3231-2011, 2011.

Auger, P. A., Ulses, C., Estournel, C., Stemmann, L., Somot, S., and Diaz, F.: Interannual control of plankton communities by deep winter mixing and prey/predator interactions in the NW Mediterranean: Results from a 30-year 3D modeling study, Prog. Oceanogr., 124, 12–27, https://doi.org/10.1016/j.pocean.2014.04.004, 2014.

Brasseur, P., Beckers, J. M., Brankart, J. M., and Schoenauer, R.: Seasonal temperature and salinity fields in the Mediterranean Sea: Climatological analyses of a historical data set, Deep Sea Res. Part Oceanogr. Res. Pap., 43, 159–192, https://doi.org/10.1016/0967-0637(96)00012-X, 1996.

Christaki, U., Courties, C., Karayanni, H., Giannakourou, A., Maravelias, C., Kormas, K. Ar., and Lebaron, P.: Dynamic Characteristics of Prochlorococcus and Synechococcus Consumption by Bacterivorous Nanoflagellates, Microb. Ecol., 43, 341–352, https://doi.org/10.1007/s00248-002-2002-3, 2002.

Christaki, U., Van Wambeke, F., Lefevre, D., Lagaria, A., Prieur, L., Pujo-Pay, M., Grattepanche, J.-D., Colombet, J., Psarra, S., Dolan, J. R., Sime-Ngando, T., Conan, P., Weinbauer, M. G., and Moutin, T.: Microbial food webs and

https://doi.org/10.5194/egusphere-2025-4028
Preprint. Discussion started: 16 September 2025

623 metabolic state across oligotrophic waters of the Mediterranean Sea during summer, Biogeosciences, 8, 1839–1852,
624 https://doi.org/10.5194/bg-8-1839-2011, 2011.

625 Conan, P. and Durrieu De Madron, X.: PERLE2 cruise, Pourquoi pas ? R/V, https://doi.org/10.17600/18000865, 2019.

626 Copin-Montégut, C. and Bégovic, M.: Distributions of carbonate properties and oxygen along the water column (0–
627 2000m) in the central part of the NW Mediterranean Sea (Dyfamed site): influence of winter vertical mixing on air–
628 sea CO2 and O2 exchanges, Deep Sea Res. Part II Top. Stud. Oceanogr., 49, 2049–2066,
629 https://doi.org/10.1016/S0967-0645(02)00027-9, 2002.

630 Coppola, L., Prieur, L., Taupier-Letage, I., Estournel, C., Testor, P., Lefevre, D., Belamari, S., LeReste, S., and
631 Taillandier, V.: Observation of oxygen ventilation into deep waters through targeted deployment of multiple A rgo-
632 O_2 floats in the north-western Mediterranean Sea in 2013, J. Geophys. Res. Oceans, 122, 6325–6341,
633 https://doi.org/10.1002/2016JC012594, 2017.

634 Coppola, L., Legendre, L., Lefevre, D., Prieur, L., Taillandier, V., and Diamond Riquier, E.: Seasonal and inter-annual
635 variations of dissolved oxygen in the northwestern Mediterranean Sea (DYFAMED site), Prog. Oceanogr., 162, 187–
636 201, https://doi.org/10.1016/j.pocean.2018.03.001, 2018.

637 Cossarini, G., Feudale, L., Teruzzi, A., Bolzon, G., Coidessa, G., Solidoro, C., Di Biagio, V., Amadio, C., Lazzari, P.,
638 Brosich, A., and Salon, S.: High-Resolution Reanalysis of the Mediterranean Sea Biogeochemistry (1999–2019),
639 Front. Mar. Sci. 8, 741486, https://doi.org/10.3389/fmars.2021.741486, 2021.

640 Damien, P., Bosse, A., Testor, P., Marsaleix, P., and Estournel, C.: Modeling Postconvective Submesoscale Coherent
641 Vortices in the Northwestern Mediterranean Sea, J. Geophys. Res. Oceans, 122, 9937–9961,
642 https://doi.org/10.1002/2016JC012114, 2017.

643 Di Biagio, V., Salon, S., Feudale, L., and Cossarini, G.: Subsurface oxygen maximum in oligotrophic marine
644 ecosystems: mapping the interaction between physical and biogeochemical processes, https://doi.org/10.5194/bg-
645 2022-70, 8 April 2022.

646 D'Ortenzio, F. and Ribera d'Alcalà, M.: On the trophic regimes of the Mediterranean Sea: a satellite analysis,
647 Biogeosciences, 6, 139–148, https://doi.org/10.5194/bg-6-139-2009, 2009.

648 D'Ortenzio, F., Antoine, D., and Marullo, S.: Satellite-driven modeling of the upper ocean mixed layer and air–sea
649 CO2 flux in the Mediterranean Sea, Deep Sea Res. Part Oceanogr. Res. Pap., 55, 405–434,
650 https://doi.org/10.1016/j.dsr.2007.12.008, 2008.

651 D'Ortenzio, F., Taillandier, V., Claustre, H., Coppola, L., Conan, P., Dumas, F., Durrieu Du Madron, X., Fourrier,
652 M., Gogou, A., Karageorgis, A., Lefevre, D., Leymarie, E., Oviedo, A., Pavlidou, A., Poteau, A., Poulain, P. M.,
653 Prieur, L., Psarra, S., Puyo-Pay, M., Ribera d'Alcalà, M., Schmechtig, C., Terrats, L., Velaoras, D., Wagener, T., and
654 Wimart-Rousseau, C.: BGC-Argo Floats Observe Nitrate Injection and Spring Phytoplankton Increase in the Surface
655 Layer of Levantine Sea (Eastern Mediterranean), Geophys. Res. Lett., 48, e2020GL091649,
656 https://doi.org/10.1029/2020GL091649, 2021.

https://doi.org/10.5194/egusphere-2025-4028
Preprint. Discussion started: 16 September 2025

657 Escudier, R., Clementi, E., Cipollone, A., Pistoia, J., Drudi, M., Grandi, A., Lyubartsev, V., Lecci, R., Aydogdu, A.,
658 Delrosso, D., Omar, M., Masina, S., Coppini, G., and Pinardi, N.: A High Resolution Reanalysis for the Mediterranean
659 Sea, Front. Earth Sci., 9, 702285, https://doi.org/10.3389/feart.2021.702285, 2021.

660 Estournel, C., Kondrachoff, V., Marsaleix, P., and Vehil, R.: The plume of the Rhone: numerical simulation and
661 remote sensing, Cont. Shelf Res., 17, 899–924, https://doi.org/10.1016/S0278-4343(96)00064-7, 1997.

662 Estournel, C., Broche, P., Marsaleix, P., Devenon, J.-L., Auclair, F., and Vehil, R.: The Rhone River Plume in
663 Unsteady Conditions: Numerical and Experimental Results, Estuar. Coast. Shelf Sci., 53, 25–38,
664 https://doi.org/10.1006/ecss.2000.0685, 2001.

665 Estournel, C., Zervakis, V., Marsaleix, P., Papadopoulos, A., Auclair, F., Perivoliotis, L., and Tragou, E.: Dense water
666 formation and cascading in the Gulf of Thermaikos (North Aegean), from observations and modelling, Cont. Shelf
667 Res., 25, 2366–2386, https://doi.org/10.1016/j.csr.2005.08.014, 2005.

668 Estournel, C., Testor, P., Damien, P., D'Ortenzio, F., Marsaleix, P., Conan, P., Kessouri, F., Durrieu De Madron, X.,
669 Coppola, L., Lellouche, J., Belamari, S., Mortier, L., Ulses, C., Bouin, M., and Prieur, L.: High resolution modeling
670 of dense water formation in the north-western Mediterranean during winter 2012–2013: Processes and budget, J.
671 Geophys. Res. Oceans, 121, 5367–5392, https://doi.org/10.1002/2016JC011935, 2016.

672 Estournel, C., Marsaleix, P., and Ulses, C.: A new assessment of the circulation of Atlantic and Intermediate Waters
673 in the Eastern Mediterranean, Prog. Oceanogr., 198, 102673, https://doi.org/10.1016/j.pocean.2021.102673, 2021.

674 Fourrier, M.: Dataset used for CANYON-MED training and validation,
675 https://doi.org/10.6084/M9.FIGSHARE.12452795.V2, 2020.

676 Fourrier, M., Coppola, L., D'Ortenzio, F., Migon, C., and Gattuso, J.: Impact of Intermittent Convection in the
677 Northwestern Mediterranean Sea on Oxygen Content, Nutrients, and the Carbonate System, J. Geophys. Res. Oceans,
678 127, e2022JC018615, https://doi.org/10.1029/2022JC018615, 2022.

679 Gačić, M., Borzelli, G. L. E., Civitarese, G., Cardin, V., and Yari, S.: Can internal processes sustain reversals of the
680 ocean upper circulation? The Ionian Sea example, Geophys. Res. Lett., 37, 2010GL043216,
681 https://doi.org/10.1029/2010GL043216, 2010.

682 Garinet, A., Herrmann, M., Marsaleix, P., and Pénicaud, J.: Spurious numerical mixing under strong tidal forcing: a
683 case study in the south-east Asian seas using the Symphonie model (v3.1.2), Geosci. Model Dev., 17, 6967–6986,
684 https://doi.org/10.5194/gmd-17-6967-2024, 2024.

685 Grégoire, M., Raick, C., and Soetaert, K.: Numerical modeling of the central Black Sea ecosystem functioning during
686 the eutrophication phase, Prog. Oceanogr., 76, 286–333, https://doi.org/10.1016/j.pocean.2008.01.002, 2008.

687 Grégoire, M., Garçon, V., Garcia, H., Breitburg, D., Isensee, K., Oschlies, A., Telszewski, M., Barth, A., Bittig, H.
688 C., Carstensen, J., Carval, T., Chai, F., Chavez, F., Conley, D., Coppola, L., Crowe, S., Currie, K., Dai, M., Deflandre,
689 B., Dewitte, B., Diaz, R., Garcia-Robledo, E., Gilbert, D., Giorgetti, A., Glud, R., Gutierrez, D., Hosoda, S., Ishii, M.,
690 Jacinto, G., Langdon, C., Lauvset, S. K., Levin, L. A., Limburg, K. E., Mehrtens, H., Montes, I., Naqvi, W., Paulmier,

https://doi.org/10.5194/egusphere-2025-4028
Preprint. Discussion started: 16 September 2025

A., Pfeil, B., Pitcher, G., Pouliquen, S., Rabalais, N., Rabouille, C., Recape, V., Roman, M., Rose, K., Rudnick, D., Rummer, J., Schmechtig, C., Schmidtko, S., Seibel, B., Slomp, C., Sumalia, U. R., Tanhua, T., Thierry, V., Uchida, H., Wanninkhof, R., and Yasuhara, M.: A Global Ocean Oxygen Database and Atlas for Assessing and Predicting Deoxygenation and Ocean Health in the Open and Coastal Ocean, Front. Mar. Sci., 8, 724913, https://doi.org/10.3389/fmars.2021.724913, 2021.

Habib, J., Ulses, C., Estournel, C., Fakhri, M., Marsaleix, P., Pujo-Pay, M., Fourrier, M., Coppola, L., Mignot, A., Mortier, L., and Conan, P.: Seasonal and interannual variability of the pelagic ecosystem and of the organic carbon budget in the Rhodes Gyre (eastern Mediterranean): influence of winter mixing, Biogeosciences, 20, 3203–3228, https://doi.org/10.5194/bg-20-3203-2023, 2023.

Hainbucher, D., Álvarez, M., Astray Uceda, B., Bachi, G., Cardin, V., Celentano, P., Chaikakis, S., Chavez Montero, M. D. M., Civitarese, G., Fajar, N. M., Fripiat, F., Gerke, L., Gogou, A., Fernández Guallart, E., Gülk, B., Hassoun, A. E. R., Lange, N., Rochner, A., Santinelli, C., Steinhoff, T., Tanhua, T., Urbini, L., Velaoras, D., Wolf, F., and Welsch, A.: Variability and Trends in Physical and Biogeochemical Parameters of the Mediterranean Sea during a Cruise with RV MARIA S. MERIAN in March 2018, https://doi.org/10.5194/essd-2020-82, 7 July 2020.

Helm, K. P., Bindoff, N. L., and Church, J. A.: Observed decreases in oxygen content of the global ocean: GLOBAL DECREASES IN OCEAN OXYGEN LEVELS, Geophys. Res. Lett., 38, n/a-n/a, https://doi.org/10.1029/2011GL049513, 2011.

Herrmann, M., Somot, S., Sevault, F., Estournel, C., and Déqué, M.: Modeling the deep convection in the northwestern Mediterranean Sea using an eddy-permitting and an eddy-resolving model: Case study of winter 1986–1987, J. Geophys. Res. Oceans, 113, 2006JC003991, https://doi.org/10.1029/2006JC003991, 2008.

Herrmann, M., Diaz, F., Estournel, C., Marsaleix, P., and Ulses, C.: Impact of atmospheric and oceanic interannual variability on the Northwestern Mediterranean Sea pelagic planktonic ecosystem and associated carbon cycle: Interannual Variability Impact on Nwms, J. Geophys. Res. Oceans, 118, 5792–5813, https://doi.org/10.1002/jgrc.20405, 2013.

Houpert, L., Testor, P., Durrieu De Madron, X., Somot, S., D'Ortenzio, F., Estournel, C., and Lavigne, H.: Seasonal cycle of the mixed layer, the seasonal thermocline and the upper-ocean heat storage rate in the Mediterranean Sea derived from observations, Prog. Oceanogr., 132, 333–352, https://doi.org/10.1016/j.pocean.2014.11.004, 2015.

Kessouri, F., Ulses, C., Estournel, C., Marsaleix, P., Severin, T., Pujo-Pay, M., Caparros, J., Raimbault, P., Pasqueron De Fommervault, O., D'Ortenzio, F., Taillandier, V., Testor, P., and Conan, P.: Nitrogen and Phosphorus Budgets in the Northwestern Mediterranean Deep Convection Region, J. Geophys. Res. Oceans, 122, 9429–9454, https://doi.org/10.1002/2016JC012665, 2017.

Kessouri, F., Ulses, C., Estournel, C., Marsaleix, P., D'Ortenzio, F., Severin, T., Taillandier, V., and Conan, P.: Vertical Mixing Effects on Phytoplankton Dynamics and Organic Carbon Export in the Western Mediterranean Sea, J. Geophys. Res. Oceans, 123, 1647–1669, https://doi.org/10.1002/2016JC012669, 2018.

https://doi.org/10.5194/egusphere-2025-4028
Preprint. Discussion started: 16 September 2025

Klein, B., Roether, W., Kress, N., Manca, B. B., Ribera d'Alcala, M., Souvermezoglou, E., Theocharis, A., Civitarese, G., and Luchetta, A.: Accelerated oxygen consumption in eastern Mediterranean deep waters following the recent changes in thermohaline circulation, J. Geophys. Res. Oceans, 108, 2002JC001454, https://doi.org/10.1029/2002JC001454, 2003.

Körtzinger, A., Schimanski, J., Send, U., and Wallace, D.: The Ocean Takes a Deep Breath, Science, 306, 1337–1337, https://doi.org/10.1126/science.1102557, 2004.

Körtzinger, A., Send, U., Lampitt, R. S., Hartman, S., Wallace, D. W. R., Karstensen, J., Villagarcia, M. G., Llinás, O., and DeGrandpre, M. D.: The seasonal p CO_2 cycle at 49°N/16.5°W in the northeastern Atlantic Ocean and what it tells us about biological productivity, J. Geophys. Res. Oceans, 113, 2007JC004347, https://doi.org/10.1029/2007JC004347, 2008.

Kress, N. and Herut, B.: Spatial and seasonal evolution of dissolved oxygen and nutrients in the Southern Levantine Basin (Eastern Mediterranean Sea): chemical characterization of the water masses and inferences on the N:P ratios, Deep Sea Res. Part Oceanogr. Res. Pap., 48, 2347–2372, https://doi.org/10.1016/S0967-0637(01)00022-X, 2001.

Kress, N., Manca, B. B., Klein, B., and Deponte, D.: Continuing influence of the changed thermohaline circulation in the eastern Mediterranean on the distribution of dissolved oxygen and nutrients: Physical and chemical characterization of the water masses, J. Geophys. Res. Oceans, 108, 2002JC001397, https://doi.org/10.1029/2002JC001397, 2003.

Kress, N., Gertman, I., and Herut, B.: Temporal evolution of physical and chemical characteristics of the water column in the Easternmost Levantine basin (Eastern Mediterranean Sea) from 2002 to 2010, J. Mar. Syst., 135, 6–13, https://doi.org/10.1016/j.jmarsys.2013.11.016, 2014.

Lagaria, A., Psarra, S., Lefèvre, D., Van Wambeke, F., Courties, C., Pujo-Pay, M., Oriol, L., Tanaka, T., and Christaki, U.: The effects of nutrient additions on particulate and dissolved primary production and metabolic state in surface waters of three Mediterranean eddies, Biogeosciences, 8, 2595–2607, https://doi.org/10.5194/bg-8-2595-2011, 2011.

Lascaratos, A. and Nittis, K.: A high-resolution three-dimensional numerical study of intermediate water formation in the Levantine Sea, J. Geophys. Res. Oceans, 103, 18497–18511, https://doi.org/10.1029/98JC01196, 1998.

Lascaratos, A., Roether, W., Nittis, K., and Klein, B.: Recent changes in deep water formation and spreading in the eastern Mediterranean Sea: a review, Prog. Oceanogr., 44, 5–36, https://doi.org/10.1016/S0079-6611(99)00019-1, 1999.

Lavigne, H., D'Ortenzio, F., Migon, C., Claustre, H., Testor, P., d'Alcalà, M. R., Lavezza, R., Houpert, L., and Prieur, L.: Enhancing the comprehension of mixed layer depth control on the Mediterranean phytoplankton phenology: Mediterranean Phytoplankton Phenology, J. Geophys. Res. Oceans, 118, 3416–3430, https://doi.org/10.1002/jgrc.20251, 2013.

Lavigne, H., D'Ortenzio, F., Ribera D'Alcalà, M., Claustre, H., Sauzède, R., and Gacic, M.: On the vertical distribution of the chlorophyll a concentration in the Mediterranean Sea: a basin-scale and seasonal approach, Biogeosciences, 12, 5021–5039, https://doi.org/10.5194/bg-12-5021-2015, 2015.

https://doi.org/10.5194/egusphere-2025-4028
Preprint. Discussion started: 16 September 2025

760 Legendre, L. and Rassoulzadegan, F.: Plankton and nutrient dynamics in marine waters, Ophelia, 41, 153–172,
761 https://doi.org/10.1080/00785236.1995.10422042, 1995.

762 Malanotte-Rizzoli, P., Manca, B. B., Marullo, S., Ribera D' Alcala', M., Roether, W., Theocharis, A., Bergamasco,
763 A., Budillon, G., Sansone, E., Civitarese, G., Conversano, F., Gertman, I., Hernt, B., Kress, N., Kioroglou, S.,
764 Kontoyannis, H., Nittis, K., Klein, B., Lascaratos, A., Latif, M. A., Ozsoy, E., Robinson, A. R., Santoleri, R., Viezzoli,
765 D., and Kovacevic, V.: The Levantine Intermediate Water Experiment (LIWEX) Group: Levantine basin—A
766 laboratory for multiple water mass formation processes, J. Geophys. Res. Oceans, 108, 2002JC001643,
767 https://doi.org/10.1029/2002JC001643, 2003.

768 Malanotte-Rizzoli, P., Artale, V., Borzelli-Eusebi, G. L., Brenner, S., Crise, A., Gacic, M., Kress, N., Marullo, S.,
769 Ribera d'Alcalà, M., Sofianos, S., Tanhua, T., Theocharis, A., Alvarez, M., Ashkenazy, Y., Bergamasco, A., Cardin,
770 V., Carniel, S., Civitarese, G., D'Ortenzio, F., Font, J., Garcia-Ladona, E., Garcia-Lafuente, J. M., Gogou, A.,
771 Gregoire, M., Hainbucher, D., Kontoyannis, H., Kovacevic, V., Kraskapoulou, E., Kroskos, G., Incarbona, A.,
772 Mazzocchi, M. G., Orlic, M., Ozsoy, E., Pascual, A., Poulain, P.-M., Roether, W., Rubino, A., Schroeder, K., Siokou-
773 Frangou, J., Souvermezoglou, E., Sprovieri, M., Tintoré, J., and Triantafyllou, G.: Physical forcing and
774 physical/biochemical variability of the Mediterranean Sea: a review of unresolved issues and directions for future
775 research, Ocean Sci., 10, 281–322, https://doi.org/10.5194/os-10-281-2014, 2014.

776 Manca, B., Burca, M., Giorgetti, A., Coatanoan, C., Garcia, M.-J., and Iona, A.: Physical and biochemical averaged
777 vertical profiles in the Mediterranean regions: an important tool to trace the climatology of water masses and to
778 validate incoming data from operational oceanography, J. Mar. Syst., 48, 83–116,
779 https://doi.org/10.1016/j.jmarsys.2003.11.025, 2004.

780 Many, G., Ulses, C., Estournel, C., and Marsaleix, P.: Particulate organic carbon dynamics in the Gulf of Lion shelf
781 (NW Mediterranean) using a coupled hydrodynamic–biogeochemical model, Biogeosciences, 18, 5513–5538,
782 https://doi.org/10.5194/bg-18-5513-2021, 2021.

783 Marsaleix, P., Estournel, C., Kondrachoff, V., and Vehil, R.: A numerical study of the formation of the Rhône River
784 plume, J. Mar. Syst., 14, 99–115, https://doi.org/10.1016/S0924-7963(97)00011-0, 1998.

785 Marsaleix, P., Auclair, F., and Estournel, C.: Considerations on Open Boundary Conditions for Regional and Coastal
786 Ocean Models, J. Atmospheric Ocean. Technol., 23, 1604–1613, https://doi.org/10.1175/JTECH1930.1, 2006.

787 Marsaleix, P., Auclair, F., Floor, J. W., Herrmann, M. J., Estournel, C., Pairaud, I., and Ulses, C.: Energy conservation
788 issues in sigma-coordinate free-surface ocean models, Ocean Model., 20, 61–89,
789 https://doi.org/10.1016/j.ocemod.2007.07.005, 2008.

790 Martínez-Pérez, A. M., Osterholz, H., Nieto-Cid, M., Álvarez, M., Dittmar, T., and Álvarez-Salgado, X. A.: Molecular
791 composition of dissolved organic matter in the Mediterranean Sea, Limnol. Oceanogr., 62, 2699–2712,
792 https://doi.org/10.1002/lno.10600, 2017.

793 Mavropoulou, A.-M., Vervatis, V., and Sofianos, S.: Dissolved oxygen variability in the Mediterranean Sea, J. Mar.
794 Syst., 208, 103348, https://doi.org/10.1016/j.jmarsys.2020.103348, 2020.

https://doi.org/10.5194/egusphere-2025-4028
Preprint. Discussion started: 16 September 2025

Mayot, N., D'Ortenzio, F., Ribera d'Alcalà, M., Lavigne, H., and Claustre, H.: Interannual variability of the Mediterranean trophic regimes from ocean color satellites, Biogeosciences, 13, 1901–1917, https://doi.org/10.5194/bg-13-1901-2016, 2016.

Mikolajczak, G., Estournel, C., Ulses, C., Marsaleix, P., Bourrin, F., Martín, J., Pairaud, I., Puig, P., Leredde, Y., Many, G., Seyfried, L., and Durrieu De Madron, X.: Impact of storms on residence times and export of coastal waters during a mild autumn/winter period in the Gulf of Lion, Cont. Shelf Res., 207, 104192, https://doi.org/10.1016/j.csr.2020.104192, 2020.

Millot, C. and Taupier-Letage, I.: Circulation in the Mediterranean Sea, in: The Mediterranean Sea, vol. 5K, edited by: Saliot, A., Springer Berlin Heidelberg, Berlin, Heidelberg, 29–66, https://doi.org/10.1007/b107143, 2005.

Ozer, T., Gertman, I., Kress, N., Silverman, J., and Herut, B.: Interannual thermohaline (1979–2014) and nutrient (2002–2014) dynamics in the Levantine surface and intermediate water masses, SE Mediterranean Sea, Glob. Planet. Change, 151, 60–67, https://doi.org/10.1016/j.gloplacha.2016.04.001, 2016.

Ozer, T., Gertman, I., Gildor, H., Goldman, R., and Herut, B.: Evidence for recent thermohaline variability and processes in the deep water of the Southeastern Levantine Basin, Mediterranean Sea, Deep Sea Res. Part II Top. Stud. Oceanogr., 171, 104651, https://doi.org/10.1016/j.dsr2.2019.104651, 2020.

Ozer, T., Rahav, E., Gertman, I., Sisma-Ventura, G., Silverman, J., and Herut, B.: Relationship between thermohaline and biochemical patterns in the levantine upper and intermediate water masses, Southeastern Mediterranean Sea (2013–2021), Front. Mar. Sci., 9, 958924, https://doi.org/10.3389/fmars.2022.958924, 2022.

Powley, H. R., Krom, M. D., and Van Cappellen, P.: Circulation and oxygen cycling in the Mediterranean Sea: Sensitivity to future climate change: OXYGEN CYCLING IN THE MEDITERRANEAN SEA, J. Geophys. Res. Oceans, 121, 8230–8247, https://doi.org/10.1002/2016JC012224, 2016.

Regaudie-de-Gioux, A., Vaquer-Sunyer, R., and Duarte, C. M.: Patterns in planktonic metabolism in the Mediterranean Sea, 2009.

Robinson, A. R. and Golnaraghi, M.: Circulation and dynamics of the Eastern Mediterranean Sea; quasi-synoptic data-driven simulations, Deep Sea Res. Part II Top. Stud. Oceanogr., 40, 1207–1246, https://doi.org/10.1016/0967-0645(93)90068-X, 1993.

Roether, W. and Schlitzer, R.: Eastern Mediterranean deep water renewal on the basis of chlorofluoromethane and tritium data, Dyn. Atmospheres Oceans, 15, 333–354, https://doi.org/10.1016/0377-0265(91)90025-B, 1991.

Roether, W. and Well, R.: Oxygen consumption in the Eastern Mediterranean, Deep Sea Res. Part Oceanogr. Res. Pap., 48, 1535–1551, https://doi.org/10.1016/S0967-0637(00)00102-3, 2001.

Salihoğlu, İ., Saydam, C., Baştürk, Ö., Yilmaz, K., Göçmen, D., Hatipoğlu, E., and Yilmaz, A.: Transport and distribution of nutrients and chlorophyll-a by mesoscale eddies in the northeastern Mediterranean, Mar. Chem., 29, 375–390, https://doi.org/10.1016/0304-4203(90)90024-7, 1990.

https://doi.org/10.5194/egusphere-2025-4028
Preprint. Discussion started: 16 September 2025

Schlitzer, R., Roether, W., Oster, H., Junghans, H.-G., Hausmann, M., Johannsen, H., and Michelato, A.: Chlorofluoromethane and oxygen in the Eastern Mediterranean, Deep Sea Res. Part Oceanogr. Res. Pap., 38, 1531–1551, https://doi.org/10.1016/0198-0149(91)90088-W, 1991.

Schmidtko, S., Stramma, L., and Visbeck, M.: Decline in global oceanic oxygen content during the past five decades, Nature, 542, 335–339, https://doi.org/10.1038/nature21399, 2017.

Schneider, A., Tanhua, T., Roether, W., and Steinfeldt, R.: Changes in ventilation of the Mediterranean Sea during the past 25 year, Ocean Sci., 10, 1–16, https://doi.org/10.5194/os-10-1-2014, 2014.

Siokou-Frangou, I., Bianchi, M., Christaki, U., Christou, E. D., Giannakourou, A., Gotsis, O., Ignatiades, L., Pagou, K., Pitta, P., Psarra, S., Souvermezoglou, E., Van Wambeke, F., and Zervakis, V.: Carbon flow in the planktonic food web along a gradient of oligotrophy in the Aegean Sea (Mediterranean Sea), J. Mar. Syst., 33–34, 335–353, https://doi.org/10.1016/S0924-7963(02)00065-9, 2002.

Siokou-Frangou, I., Christaki, U., Mazzocchi, M. G., Montresor, M., Ribera d'Alcalá, M., Vaqué, D., and Zingone, A.: Plankton in the open Mediterranean Sea: a review, Biogeosciences, 7, 1543–1586, https://doi.org/10.5194/bg-7-1543-2010, 2010.

Sisma-Ventura, G., Yam, R., Kress, N., and Shemesh, A.: Water column distribution of stable isotopes and carbonate properties in the South-eastern Levantine basin (Eastern Mediterranean): Vertical and temporal change, J. Mar. Syst., 158, 13–25, https://doi.org/10.1016/j.jmarsys.2016.01.012, 2016.

Sisma-Ventura, G., Kress, N., Silverman, J., Gertner, Y., Ozer, T., Biton, E., Lazar, A., Gertman, I., Rahav, E., and Herut, B.: Post-eastern Mediterranean Transient Oxygen Decline in the Deep Waters of the Southeast Mediterranean Sea Supports Weakening of Ventilation Rates, Front. Mar. Sci. 7, 598686, https://doi.org/10.3389/fmars.2020.598686, 2021.

Stramma, L. and Schmidtko, S.: Spatial and Temporal Variability of Oceanic Oxygen Changes and Underlying Trends, Atmosphere-Ocean, 59, 122–132, https://doi.org/10.1080/07055900.2021.1905601, 2021.

Sur, H., Ozsoy, E., and Unluata, U.: Simultaneous deep and intermediate depth convection in the northern levantine sea, winter 1992, Oceanol. Acta, 16, 1993.

Tanhua, T.: Hydrochemistry of water samples during METEOR cruise M83/1, https://doi.org/10.1594/PANGAEA.821729, 2013.

Tanhua, T., Hainbucher, D., Schroeder, K., Cardin, V., Álvarez, M., and Civitarese, G.: The Mediterranean Sea system: a review and an introduction to the special issue, Ocean Sci., 9, 789–803, https://doi.org/10.5194/os-9-789-2013, 2013.

Theocharis, A., Georgopoulos, D., Lascaratos, A., and Nittis, K.: Water masses and circulation in the central region of the Eastern Mediterranean: Eastern Ionian, South Aegean and Northwest Levantine, 1986–1987, Deep Sea Res. Part II Top. Stud. Oceanogr., 40, 1121–1142, https://doi.org/10.1016/0967-0645(93)90064-T, 1993.

https://doi.org/10.5194/egusphere-2025-4028
Preprint. Discussion started: 16 September 2025

861 Thierry, V., Bittig, H., and The Argo-Bgc Team: Argo quality control manual for dissolved oxygen concentration,
862 Argo-BGC group, https://doi.org/10.13155/46542, 2021.

863 Tugrul, S., Besiktepe, T., and Salihoglu, I.: Nutrient exchange fluxes between the Aegean and Black Seas through the
864 Marmara Sea, Mediterr. Mar. Sci., 3, 33, https://doi.org/10.12681/mms.256, 2002.

865 Ulses, C., Estournel, C., Puig, P., Durrieu De Madron, X., and Marsaleix, P.: Dense shelf water cascading in the
866 northwestern Mediterranean during the cold winter 2005: Quantification of the export through the Gulf of Lion and
867 the Catalan margin, Geophys. Res. Lett., 35, 2008GL033257, https://doi.org/10.1029/2008GL033257, 2008.

868 Ulses, C., Auger, P. -A., Soetaert, K., Marsaleix, P., Diaz, F., Coppola, L., Herrmann, M. J., Kessouri, F., and
869 Estournel, C.: Budget of organic carbon in the North- Western Mediterranean open sea over the period 2004–2008
870 using 3-D coupled physical-biogeochemical modeling, J. Geophys. Res. Oceans, 121, 7026–7055,
871 https://doi.org/10.1002/2016JC011818, 2016.

872 Ulses, C., Estournel, C., Fourrier, M., Coppola, L., Kessouri, F., Lefèvre, D., and Marsaleix, P.: Oxygen budget of the
873 north-western Mediterranean deep- convection region, Biogeosciences, 18, 937–960, https://doi.org/10.5194/bg-18-
874 937-2021, 2021.

875 Ulses, C., Estournel, C., Marsaleix, P., Soetaert, K., Fourrier, M., Coppola, L., Lefèvre, D., Touratier, F., Goyet, C.,
876 Guglielmi, V., Kessouri, F., Testor, P., and Durrieu De Madron, X.: Seasonal dynamics and annual budget of dissolved
877 inorganic carbon in the northwestern Mediterranean deep-convection region, Biogeosciences, 20, 4683–4710,
878 https://doi.org/10.5194/bg-20-4683-2023, 2023.

879 Velaoras, D., Krokos, G., Nittis, K., and Theocharis, A.: Dense intermediate water outflow from the C retan S ea: A
880 salinity driven, recurrent phenomenon, connected to thermohaline circulation changes, J. Geophys. Res. Oceans, 119,
881 4797–4820, https://doi.org/10.1002/2014JC009937, 2014.

882 Wanninkhof, R. and McGillis, W. R.: A cubic relationship between air-sea CO_2 exchange and wind speed, Geophys.
883 Res. Lett., 26, 1889–1892, https://doi.org/10.1029/1999GL900363, 1999.

884 Wolf, M. K., Hamme, R. C., Gilbert, D., Yashayaev, I., and Thierry, V.: Oxygen Saturation Surrounding Deep Water
885 Formation Events in the Labrador Sea from Argo-O_2 Data, Glob. Biogeochem. Cycles, 32, 635–653,
886 ://doi.org/10.1002/2017GB005829, 2018.

887 Ziveri, P. and Grelaud, M.: Physical oceanography during Ángeles Alvariño cruise MedSeA2013,
888 https://doi.org/10.1594/PANGAEA.846067, 2015.

889 Zodiatis, G.: Circulation of the cretan sea-water masses (eastern mediterranean-sea), Oceanol. Acta, 16, 107–
890 114,1993.